Biomechanical evaluation of the unilateral crossbite on the asymmetrical development of the craniofacial complex. A mechano-morphological approach.

Javier Ortún-Terrazas[1*], Michael J. Fagan[2], José Cegoñino[1], Edson Illipronti-Filho[3], Amaya Pérez del Palomar[1]
[1]Group of Biomaterials, Aragon Institute of Engineering Research (I3A), University of Zaragoza, Zaragoza, Spain
[2] Medical and Biological Engineering, School of Engineering and Computer Science, University of Hull, Hull, United Kingdom
[3] School of Dentistry, Department of Stomatology, University of São Paulo, São Paulo, Brazil
* Correspondence to Dr. Javier Ortún-Terrazas. Aragon Institute of Engineering Research (I3A), School of Engineering and Architecture, University of Zaragoza, Calle María de Luna 3, 50018 Zaragoza, Spain. Tel.: +34 976 761 000 (5231) fax: +34 976 761 000 (5231). E-mail: javierortun@unizar.es

Abstract

Background and Objective: The occlusion effect on the craniofacial development is a controversial topic that has attracted the interest of many researchers but that remains unclear, mainly due to the difficulties on measure its mechanical response experimentally. This mechano-morphological relationship of the craniofacial growth is often explained by the periosteal and capsular matrices of the functional matrix hypothesis (FMH); however, its outcomes have not been analytically demonstrated yet. This computational study aims, therefore, to analytically demonstrate the mechano-morphological relationship in the craniofacial development of children with unilateral crossbite (UXB) using the finite element (FE) method.

Methods: The craniofacial complex asymmetry of ten children, five of whom exhibit UXB, was 3D-analysed and compared with the biomechanical response computed from a FE analysis of each patient's occlusion. Due to the complexity of the geometry and the multitude of contacts involved, the inherent limitations of the model were evaluated by comparing computed occlusal patterns with those recorded by an occlusal analysis on 3D printed copies.

Results: Comparison's outcomes proved the reliability of our models with just a deviation error below 6% between both approaches. Out of validation process, computational results showed that the significant elongation of mandibular branch in the contralateral side could be related to the mandibular shift and increase of thickness on the crossed side, and particularly of the posterior region. These morphological changes could be associated with periodontal overpressure (>4.7kPa) and mandibular over deformation (0.002 ε) in that side, in agreement with the periosteal matrix's principles. Furthermore, the maxilla's transversal narrowing and the elevation of the maxillary and zygomatic regions on the crossed side were statistically demonstrated and seem to be related with their respective micro displacements at occlusion, as accounted by their specific capsule matrices. Our results were consistent with those reported clinically and demonstrated analytically the mechano-morphological relationship of children's craniofacial development based on the FMH's functional matrices.

Conclusions: This study is a first step in the understanding of the occlusion's effect on the craniofacial development by computational methods. Our approach could help future engineers, researchers and clinicians to understand better the aetiology of some dental malocclusions and functional disorders improve the diagnosis or even predict the craniofacial development.

Keywords: cranio-facial development, facial asymmetry, finite element method, occlusal imbalance, unilateral crossbite

Graphical abstract

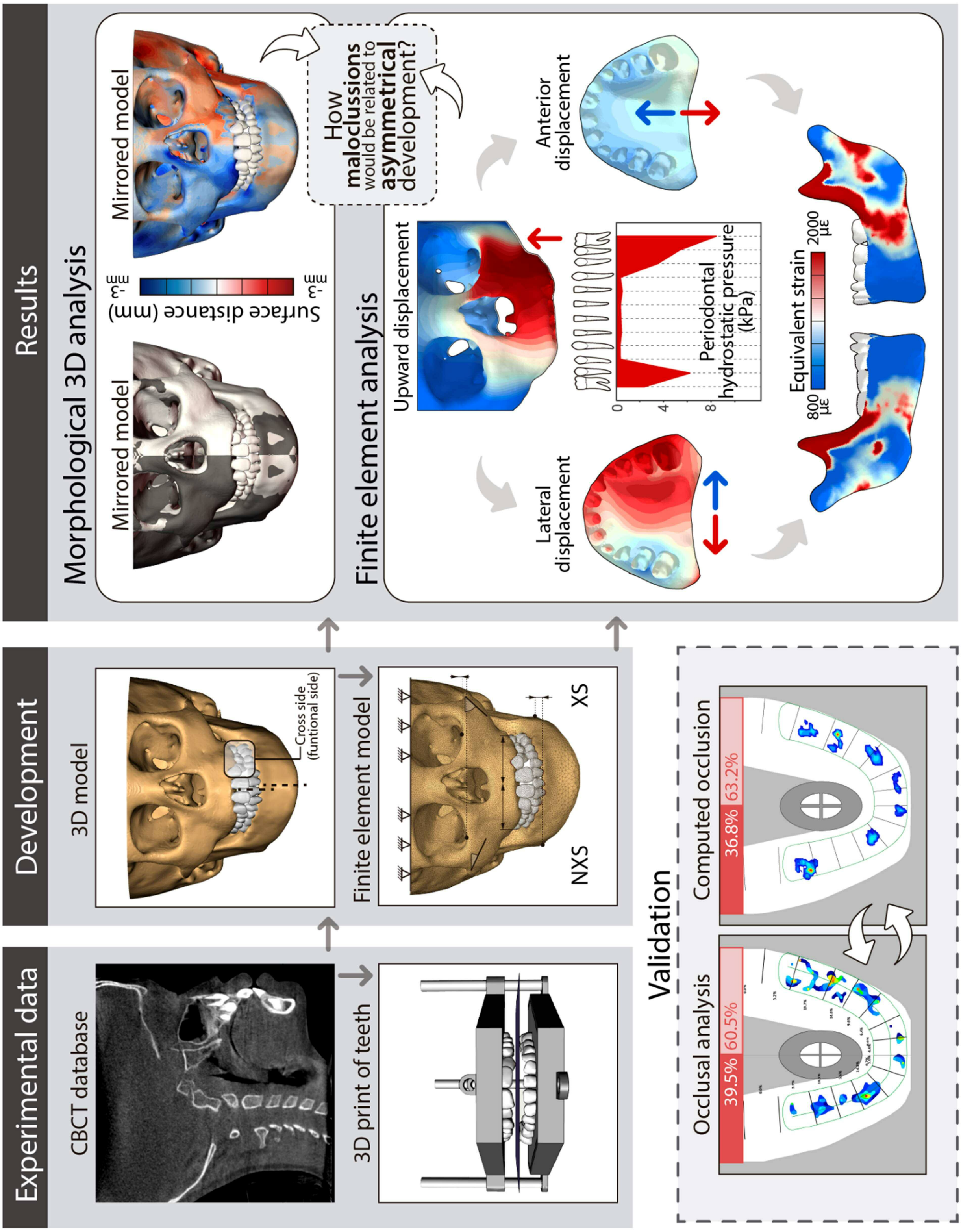

1 Introduction

The craniofacial complex is mainly composed of the cranial bones and the mandible that is bilaterally connected to the skull by the temporomandibular joints (TMJs) (Figure 1.C), the masticatory muscles (Figure 1.A) and the neurological tissues (shown in Figure 1.A). From the 1930s several theories have described the growth of the different regions of the craniofacial complex [1,2] basically according to three growth mechanisms (sutural, endochondral, and intramembranous) and two conditioning factors (genetic and environmental). Despite none theories is totally valid [2], the functional matrix hypothesis (FMH) proposed by Melvin Moss (1962) [3,4] is widely used in dental and in maxillofacial disciplines since it seems to relate the craniofacial development with the mechanical stimulus produced at the environmental activity of chewing.

Anatomically, the occlusion is guided by both TMJs and occlusal planes and its maximum force is limited by the mechanical stimuli sensed by the neural receptors, both in the soft tissues of the TMJs and in the periodontal ligaments (PDLs) (shown Figures 1.C and D). In a well-balanced occlusion, the centric occlusion coincides with the maximum intercuspation position [5] and distributes the maximum bite force almost homogeneously along all occlusal plane, avoiding harmful overloading in some regions [6]. The mechanical stimulus is therefore perceived by both mandibular nerves (shown in Figure 1.A), causing a normal and symmetrical growth. By contrast, malocclusions, such as unilateral crossbite (UXB), unbalance and gradually produce functional problems which lead to abnormal development of dental and craniofacial structures [7–9] (shown Figures 1.B and D).

UXB is characterized by the lingual occlusion of the buccal cusps of the maxillary teeth with the buccal cusps of the corresponding mandibular teeth [10] in one of the two halves (shown in Figure 1.D). Henceforth, we are going to refer to this side as the crossed side (XS), and to the opposite side as the non-crossed (NXS) side (shown in Figure 1.B). Based on the aforementioned FMH, early correction of UXB would avoid irreversible unusual development of the craniofacial complex [11,12] and painful, expensive and complex surgical treatments later in life [13]. Following this trend, some case reports and statistical studies [14,15] have tried to relate UXB with the asymmetrical adaptation of soft and hard tissues at early ages. Amongst others morphological changes observed, these studies agree in the deviation of the chin to the XS [16–18] and the width increment of the mandibular body [19] and ramus [12,20] of the same side (shown Figure 1.B). But also, the asymmetrical morphology of the maxilla [21], the abnormal development of the glenoid fosses [22,23] or the asymmetrical height of the ocular orbits and the cranial halves [24,25] were recognized. Several studies conducted on adult patients [26,27] have demonstrated that there are significant differences in the anterior and superior joint spaces, variation in thickness of the articular TMJ disc [28,29], and the anteroposterior condylar joint position in the unilateral crossbite patients [30]. Moreover, it has been found significant differences in the vertical condylar inclination, medial condylar position, condylar width and height, and volumetric joint space between the side of the unilateral occlusion and the contralateral side.

Nevertheless, none of these clinical studies have been able to establish a function-shape relationship between UXB and the asymmetrical growth [31] since they could not evaluate the mechanical stimulus sensed.

As an alternative, computational techniques [32,33], specially finite element (FE) method, have been extensively used to analyse the biomechanical effect of the occlusion into the craniofacial growth. Unfortunately, despite the numerous computational studies [31,34–36] performed, the mechano-morphological relation of the craniofacial complex is still a controversial topic. Amongst others, the unmineralized state of bones at childhood, the complex anatomy and behaviour of the tissues involved [37] or the several contacts involved [38] complicate the developing of accurate FE models at early ages. Moreover, due to these limitations, computational studies of the paediatric craniofacial complex are mainly patient-specific studies [39,40], and there are few for larger samples [41]. Fortunately, recent advances in 3D cephalometric methods, modelling commercial software, tissues engineering, and computerized occlusal analysis systems have improved its development, and consequently the knowledge about the craniofacial growth. A better knowledge of it could clarify the aetiology of some dental malocclusions and functional disorders, improve the diagnosis and treatment selection, or even help to predict the reaction after treatment.

This study aims therefore to relate the craniofacial asymmetrical growth with the mechanical stimulation computed through FE analyses of the unilateral occlusion, following the FMH's principles and using the latest advances in scanning, modelling and occlusal analysis. Hence, the maximum intercuspation occlusion was simulated in 10 detailed patient-specific FE models developed from the segmentation of Cone Beam Computed Tomography (CBCT) images of children with and without UXBs. The accuracy of these computational models was firstly checked by the comparison of the occlusal patterns computed with those recorded experimentally by an occlusal analysis system in 3D printed copies of the full dentitions. Afterwards, the occlusal patterns, the mechanical response of the tissues and the bony regions' displacements were presented and related to the asymmetrical malformations identified through a statistical and 3D-morphological comparison of both craniofacial halves. Our findings were then discussed and compared with those observed clinically in other studies of children with UXB, with a special focus on the fundamentals of the FMH. Finally, at the end of this manuscript, the potential of using FE models for the study of craniofacial growth was discussed based on our findings.

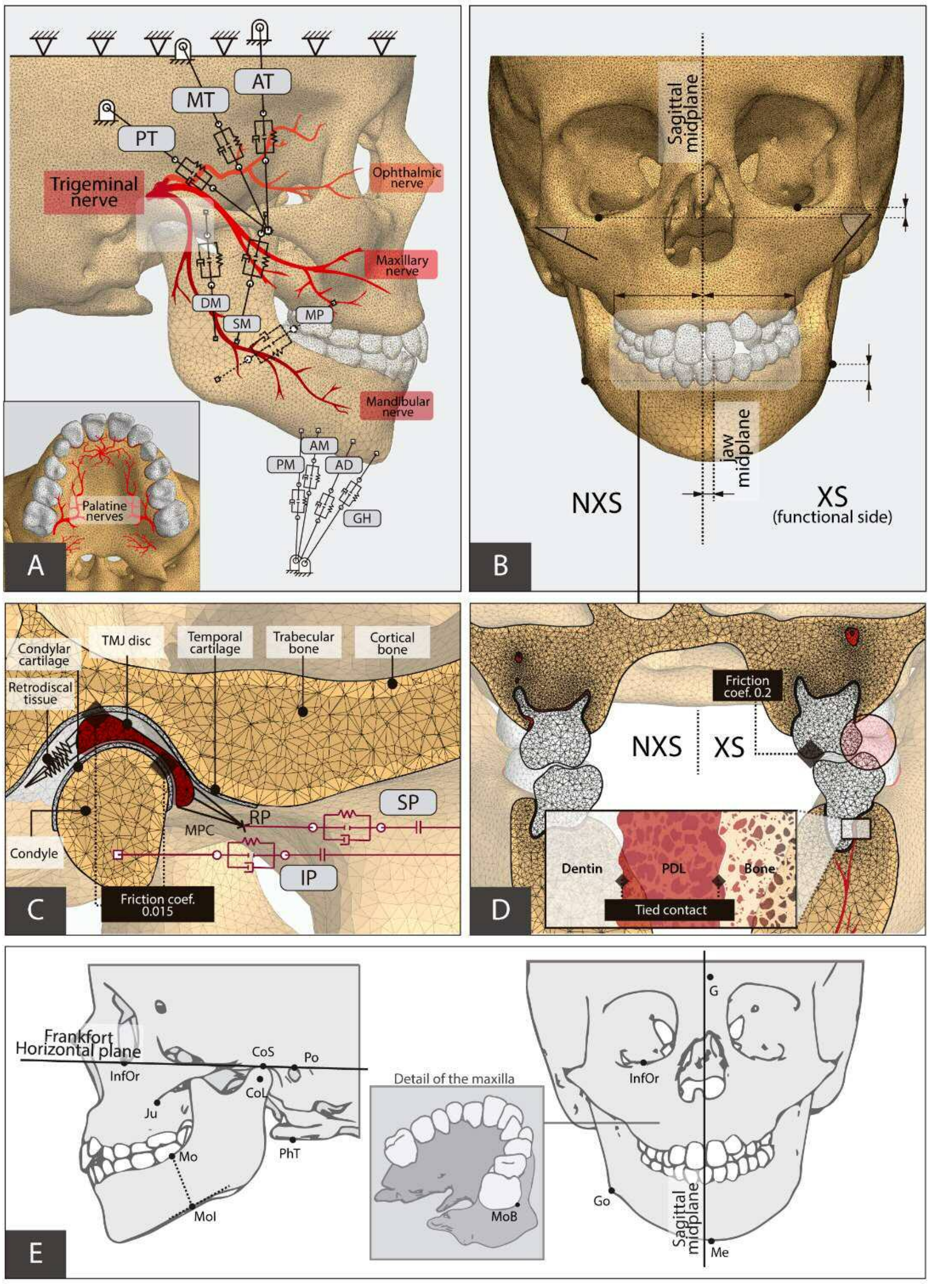

Figure 1. Captures from one of the FE models developed which show: A) a scheme of the trigeminal nerve branches, the external boundary conditions of the model and the modelling of the chewing muscles (SM, superficial masseter; DM, deep masseter; AT, anterior temporalis; MT, middle temporalis; PT, posterior temporalis; MP, medial pterygoid; IP, inferior lateral pterygoid; SP, superior lateral pterygoid; AM, anterior mylohyoid, PM, posterior mylohyoid; AD, anterior digastric and GH, geniohyoids muscle); B) some of the main morphological differences between the crossed (XS) and non-crossed side (NXS); C) the boundary conditions in the TMJ; D) the malocclusion associated to the unilateral crossbite; and the boundary conditions applied to the tooth-periodontal ligament (PDL)-bone attachment. E) Landmarks and reference planes in frontal and lateral views (landmarks' descriptions are summarized in Table 1).

2 Material and methods

2.1 FE models

Ten 3D models of the masticatory system were developed from the 3D-cephalometric images of 10 paediatric subjects with mixed dentition, three of whom exhibited left UXB and other two that have right UXB according to the diagnosis performed by an expert. To facilitate the subsequent interpretation of results, the 3D models of those patients with right UXB were mirrored with respect to the sagittal midplane, achieving to have the XS on the left side in all the subjects. This mirroring operation consisted only of a change of coordinates of the entire point cloud of the model, without altering the proportions of the facial asymmetry or the accuracy of the biomechanical simulations. On the other hand, the other five models, which constitutes the control group of this study, did not show any malocclusion or asymmetry defects. The images of UXB and control groups were respectively obtained as a part of treatment planning or of a routine medical examination through a CBCT scan system (i-CAT™; Imaging Sciences International, Hatfield, PA, USA) and all of them were scanned in a maximum intercuspation position. Data acquisition was approved by the Research Ethics Committee of the University of São Paulo – USP, School of Dentistry (numbers 200/06 and 16/2008) and subjects gave an informed consent. All datasets were obtained with an acquisition time of 5-26 s and field of view (FOV) of 13 cm × 17 cm and were output in a 14-bit greyscale and 16,384 shades of grey to a Digital Imaging and Communication in Medicine (DICOM) file through cylindrical reconstruction algorithms. The output file of each subject was composed of 210 images with an interscan distance of 0.50 mm.

To improve the limiting contours of each part in the model, a gradient filter was initially applied to each database. For the modelling of hard tissues, the images were then automatically segmented using a masking technique in the Mimics software (Mimics, v.19.; Materialise, Leuven, Belgium). This process was supervised by an expert in the radiological study of the malformations caused by UXB.

For the subsequent statistical analysis and based on our previous statistical study [42], the coordinates (x,y,z) of twelve anthropometric reference points (Table 1 and Figure 1.E) were reassessed three times by the same radiologist expert, with a month gap between each assessment. The reliability of this procedure was determined by an Intra-Class Correlation Coefficient (ICC) of 0.93. From these landmarks, 6 bilateral measurements (Table 1) were defined to study statistically the main malformations of the asymmetry.

Name	**Description**
Landmarks on sagittal midplane	
Glabella (G)	Most prominent point between the supraorbital ridges
Menton (Me)	Most inferior point in symphysis
Pharyngeal tubercle (PhT)	Lower point of the basioccipital region.
Bilateral landmarks (right and left)	
Condyle lateral (CoL)	Most lateral point of condyle head
Condyle superior (CoS)	Most superior point of condyle head
Gonion (Go)	Point between mandibular plane and ramus
Infraorbitale (InfOr)	Deepest point on infraorbital margin
Jugale (Ju)	Intersection between the margin of the frontal and temporal processes with the zygomatic bone
Last molar (Mo)	Most buccal point of the last inferior molar.
Last molar buccal (MoB)	Most buccal point of the last superior molar.
Last molar inferior (MoI)	Projection of the point on the inferior edge of the jaw.
Porion (Po)	Highest point on roof of external auditory meatus
Bilateral measurements (right and left)	
Body length	Distance between Go and Me
Body width	Distance between MoI and Mo
Condylar head width	Distance of CoS and CoL projections on the FH plane
Maxilla height	Shortest distance between Ju and the FH plane
Maxilla width	Shortest distance between MoL and the S plane
Ramus length	Distance between Go and the CoS

Table 1 Definitions of landmarks and computed bilateral measurements. Note: the distance between two landmarks was calculated by the distance formula in 3D coordinate system

For the soft tissues, cartilaginous structures, such as the articular surface which cover condyle and temporal fossa surfaces, were manually segmented by the same person as 0.2 and 0.5 mm thickness layers, respectively [43,44] (shown in Figure 1.C). It is important to highlight that just the articular layer of the condylar cartilage was modelled because of its importance from a biomechanical point of view. TMJ discs were modelled by the free space between the fibrocartilage layers having a variable thickness of about 1, 2 and 2.7 mm in intermediate, anterior, and posterior regions, in agreement with the measurements of previous studies [45] (shown in Figure 1.C). On the other hand, each PDL was modelled through Boolean subtraction operations [46]. Hence, each tooth with a positive offset (expansion) of 0.2 mm [47–49] was used to cut the maxillary bone regions. This new body was then used to define the PDL geometry through the subtraction of the normal-sized teeth (shown in Figure A.2). Further details about PDLs modelling can be found in Appendix A. Thereafter, the geometry of each tissue was parametrized using non-uniform rational bases splines-based transformation in Rhinoceros v5 software (Robert McNeel & Associates, Seattle, USA).

For the posterior comparison of results among subjects of different age and gender, 3D models were uniform scaled in order to compensate the craniofacial size differences between subjects. Hence, a linear transformation matrix [42] resulted from a Generalized Procrustes Analysis (GPA) of the patient' mandible was applied to each database. It is remarkable that the whole model's volume was not considered for the matrix computation since different cranial portions were scanned in each database, as it was widely explained in our previous publication [42]. As a result of this linear and uniform transformation, a more homogeneous sample was obtained reducing the differences due to sex and age, but without affecting the shape and proportions of each subject.

The 3D-domain of each model was meshed via a free meshing technique in Abaqus software (Abaqus 6.14, Simulia, Rhode Island, USA), resulting in meshes of around 3,102,476 second-order tetrahedral elements (C3D10-type element in Abaqus) and 6,259,966 nodes. Mesh size was determined after a mesh convergence process in which further refinement of the mesh resulted in differences of the results less than 7%. As a result of this convergence test, hard and soft tissues were respectively discretized by elements whose mean dimensions were 0.20 and 0.1 mm, respectively in all directions. In those tissues with almost incompressible behaviour, such as TMJ discs and fibrocartilage layers, hybrid formulation (C3D10H-type element in Abaqus) was included, whereas for PDLs and their adjacent trabecular tissue, the porous contribution (C3D10MP-type element in Abaqus) was added.

Following previous studies' recommendations [50–52], the effect of a collagen network embedded in the tissue's matrix was considered in the definition of TMJ discs and cartilaginous layers behaviours. Hence, the collagen fibres in these tissues were oriented anteroposteriorly in the central region and forming a ring on the periphery, dividing these tissues in five different regions (anterior, posterior, central, medial and lateral) with particular mechanical properties and fibres orientations. This complex fibres embedded behaviour was characterized by a transversally isotropic hyperelastic material model whose strain energy density function [53] is defined as follows:

$$ = {}_{1} \cdot (\tilde{}_{1} - 3) + \frac{1}{2 \cdot {}_{2}}\{ \quad [{}_{2} \cdot (\tilde{}_{4} - 1)^{2}] - 1\} + \frac{1}{\mathrm{D}}\left(\frac{({}_{el})^{2} - 1}{2} - \quad {}_{el}\right) \qquad (1)$$

where ${}_1$ is a material constant related to the ground substance; ${}_1 > 0$ and ${}_2 > 0$ are the parameters that identify the exponential behaviour due to the presence of collagen fibres; is the compressibility modulus; ${}_{el}$ is the elastic volume strain, and $\tilde{}_1$ and $\tilde{}_4$ are terms of the modified invariants that arise from uncoupling the dilatational and deviatoric responses, respectively. These invariants are defined as:

$$\tilde{}_1 = \tilde{} \qquad \tilde{}_4 = {}^0 \cdot \tilde{} \cdot {}^0 \tag{2}$$

where ^{0} is unitary vector defining the orientation of the collagen fibres and $\tilde{}$ is the modified Green tensor in the reference configuration defined by the deformation gradient $\tilde{}$, as $\tilde{}\,(\hat{}_i) = \tilde{}^T\tilde{}$. The stretch $(\hat{}_i)$ is defined as the ratio between fibre length in deformed ( ) and in reference configurations ( ) in direction .

Whereas, in the PDLs, the transversely isotropic behaviour caused by collagen fibres was neglected since the centric occlusion simulated produced mainly intrusive forces which hardly stretched the collagen fibres [49]. This compressive loading produces a viscoelastic response of the tissue, which was described in our previous models by the strain energy density function of a highly compressible isotropic hyperelastic material [54] as follows:

$$= \frac{2}{\,{}^2} \left[\hat{}_1^{\alpha} + \hat{}_2^{\alpha} + \hat{}_3^{\alpha} - 3 + \frac{1}{}\left({}_{el}^{-\alpha\beta} - 1 \right) \right] \tag{3}$$

where and are material parameters and the coefficient determines the degree of compressibility being related to Poisson's ratio, , by $= /(1-2\ )$. Considering that the PDL is a fully saturated porous tissue (Figure 1.D), the total stress, , is then defined by the second Piola-Kirchhoff stress tensor of the solid phase of the aforementioned hyperelastic material model, $\bar{}_s$, and the coupling of the fluid phase pressure [54] as follows:

$$= (1 - \ ) \cdot \bar{}_s - \ \cdot \bar{}_t \cdot \tag{4}$$

where is the porosity defined as the ratio of trapped fluid volume $(\ _f)$ to total volume $(\ _t)$ and $\bar{}_t$ is the average pressure stress of the interstitial fluid which is related to the Jacobian contribution from the permeability of the tissue by the nonlinear Forchheimer flow law. This law was employed in Abaqus to describe the fluid flow for a permeability, , which varies with the deformation by the exponential permeability function described by [55] for biphasic materials:

$$= {}_0\left[\frac{(1+{}_0)}{{}_0(1+)}\right]^2 \quad \left[\ \left(\frac{1+}{1+{}_0}-1\right)\right] \tag{5}$$

where is the void ratio related to the tissue's porosity by $= /(1-)$, ${}_0$ and ${}_0$ are the permeability and the void ratio at zero strain, and *M* is a dimensionless material parameter. To allow the fluid interaction between PDL and bone, a fluid pressure of 0.0 MPa [56] was set on the surface where PDLs are attached to the bone (shown in Figure 1.D). Table 2 summarizes the parameters of the above-mentioned material models and those that define the elastic and porous-elastic behaviour of the hard tissues.

Regarding the external boundary conditions, as it is often assumed in this kind of simulations, the upper nodes of the skull were fixed (shown in Figure 1.A) and both PDLs and cartilages were connected to the adjacent bony structures by tied contacts (Figure 1.C and D, respectively).

Muscular loads were applied as contractile forces using connector elements (CONN3D2-type element in Abaqus) which reproduced the passive, active and damping behaviour of the muscles (shown in Figure 1.A). For the infant participants of this study, these forces were approximated from adult measurements by considering a lower maximum bite force at childhood than at adulthood. Moreover, for those subjects with UXB, the muscles' forces and the ^{i} values in each side have been adapted for considering respectively -20% [57] and -5% [58] asymmetry indexes. The full process to compute muscular components and the resultant contractile forces are fully detailed in the appendix B. These contractile forces were gradually applied for 1.6 seconds mimicking the muscles contraction at maximum intercuspation occlusion. However, the numerical results were not been captured until 2.76 seconds in order to simulate the time dependent reactions of the soft tissues at clenching [59].

Table 2. Mechanical properties assigned to each region of the FE model. E, elastic modulus; , Poisson coefficient; $_w$, specific weight of the interstitial fluid.

Elastic material model

Region	(MPa)	(-)
Cortical bone[(a)]	20000	0.30
Dentin[(b)]	15000	0.31

Transversally isotropic material model

Region	$_1$ (MPa)	(MPa^{-1})	$_1$ (MPa)	$_2$ (-)
TMJ disc (boys)[(c)]				
Anterior	1.45	0	0.43	0.34
Lateral	1.45	0	0.69	0.43
Central	1.45	0	0.97	0.17
Medial	1.45	0	0.17	1.68
Posterior	1.45	0	1.25	0.16
TMJ disc (girls)[(c)]				
Anterior	2.4	0	0.05	3.72
Lateral	2.4	0	0.11	2.52
Central	2.4	0	0.75	0.87
Medial	2.4	0	0.08	2.93
Posterior	2.4	0	0.31	1.44
Cartilages[(c)]				
Anterior	1.65	0	0.24	1.95
Lateral	1.65	0	2.58	0.43
Central	1.65	0	3.77	0.21
Medial	1.65	0	2.52	0.42
Posterior	1.65	0	0.16	1.92

Porous elastic material model

	Solid phase		*Porous phase*			
Region	(MPa)	(-)	$_0 \cdot 10^{-15}$ (m^2)	(-)	$_0$ (-)	$_w$ (N/m^3)
Trabecular bone[(b)]	345	0.31	52.9	-	4	9800

Porous hyperfoam material model

	Solid phase			*Porous phase*			
Region	(MPa)	(-)	(-)	$_0 \cdot 10^{-15}$ (m^2)	(-)	$_0$ (-)	$_w$ (N/m^3)
PDL [(b)]	0.03	20.9	0.257	8.81	14.2	2.33	9800

a) Lacroix and Prendergast, 2002 [60].
b) Bergomi et al., 2011 [56].
c) Ortún-Terrazas et al., 2020 [61].

It is also noteworthy that the insertion of the superior portion of lateral pterygoid in a unique node of the TMJ disc would cause an excessive distortion of the adjacent elements of the disc. For avoiding it, the superficial nodes of the anterior disc band were connected to an intermediate reference point by several multipoint constraint elements (MPC) and then to the muscle insertion (shown in Figure 1.C). On the other hand, the TMJ disc posterior attachment was modelled by spring elements (shown in Figure 1.C) of 0.008 N/mm stiffness, as in an elsewhere study [62]. Finally, the sliding contacts between teeth and disc-cartilages were defined respectively by friction coefficients of 0.2 [63], and 0.015 [64] using a penalty formulation (Figures 1.D and C).

2.2 Occlusal analysis by T-Scan

The dental cusps reconstructed were then assembled on two thin sheets of 0.5 mm thickness (shown in Figure C.1) and exported through the slicer software (Ultimaker Cura 3.6.0, Geldermalsen, Netherlands) to the desktop printer Ultimaker 3 (Ultimaker B.V., the Netherlands) for 3D-printing (layer height: 0.06 mm; wall thickness: 1 mm; infill density: 40%; speed: 60 mm/s; temperature: 195 °C). For printing the dental arches and their respective external holders, Polylactic Acid (PLA-Ultimaker BV, Geldermalsen, Netherlands) material ($= 2346.5$) was used. The inferior holder was fixed in the assembly, while the superior one could just move vertically (shown in Figure C.1.A of the appendix C) since, as described in the previous section, the initial position of the model was already situated at maximum intercuspation, and it is just necessary a minimal vertical displacement to contact both dental arches.

To perform the experimental test, a piezoelectric film sensor was introduced between the 3D printed superior and inferior teeth arcades. This sensor records the occlusal contacts at maximum intercuspation by means of a T-Scan III system (Tek-Scan South Boston, MA, USA) (the assembly can be seen in Figure C.1). The piezoelectric film was a 100-μm-thick mylar-encased recording sensor with 1500 compressible sensitive receptor points and was inserted into a plastic U-shaped device. The U-shaped device was positioned parallel to the upper occlusal plane and centred along the midline between the upper central incisor teeth by a dentist with expertise in occlusal analysis. Then, a 2-kg-weight was applied to the superior component of the assembly to record the normalized contact pressures. The load value was computed by an inverse FE analysis in a way that the stress did not produce a noticeable deformation (minimum principal strain $< 0.01\ \varepsilon$) on the printed samples which could modify the occlusal plane. Apart from avoiding occlusal malformations, the load's magnitude had not a quantifiable effect on the results recorded by the T-Scan III system, since the system computed just the relative percentage of the total contact load recorded. This procedure was repeated three times for each case in order to check the sensitivity of the test. Afterwards, the occlusal patterns recorded were plotted in the T-Scan v10 software, as can be seen in Figure 2.

On the other hand, as it had been conducted in our previous study [59], the contact pressures in the computational models were recorded using a virtual square-shape film of 0.1 mm thickness positioned as in the experimental test. This virtual film was composed of 7,200 second-order quadrilateral membrane elements (M3D8-type element in Abaqus) and its behaviour was defined based on the linear elastic properties of Mylar840 material (DuPont; = 5 and = 0.3). With the upper nodes of the skull fixed, the contractile forces described in section 2.1 were applied to the model. Although the models were initially placed in the maximum intercuspation position, muscular forces were needed to engage the occlusal pattern on the virtual film. Finally, to display the relative percentages computed as those measured by the T-Scan III system, a 3D bars graph was developed in MATLAB (MATLAB 6.0 R12 The MathWorks Inc., Natick, MA, 2000). The height of the bars in this graph shows the contact pressure in the centroid of each film-element, while the width and depth represent its location in the reticule of the virtual film (80 x 90 elements). Both contact and location data were firstly extracted from Abaqus' output file through a Python script ("Python 3.5.2, Python Software Foundation").

2.3 Morphological and statistical 3D-analysis

The first step of this morphological analysis was, therefore, to define an appropriate sagittal midplane [65] which divides the craniofacial complex by compensating any asymmetrical variations. Thus, a new model was symmetrically copied from an approximate midplane which had been defined by the midpoints of the glabella, menton and pharyngeal tubercle. The mirrored model was then aligned to the original one through applying the Iterative Closest Point (ICP) algorithm. The combination of these point clouds, original and mirrored ones, provided an ideal symmetrical model of the patient whose first three eigenvectors established the desired sagittal midplane [42]. Eigenvectors of this idealized model were then computed through Principal Component Analysis (PCA) of the points that constituted the 3D model. As a result, this midplane was used to build a new mirrored model which serve to compute the normal distance with the original model, i.e. to compute the morphological differences between both hemifacial sides. All these operations were performed in MATLAB, while the plotting of normal distances was displayed in Paraview software (Paraview v5.6, National Technology & Engineering Solutions of Sandia, New Mexico). On the other hand, for the statistical study, the differences between the 6 bilateral measurements of both halves were tested by a Mann-Whitney U test (significance level ≤ 0.05) in both groups and halves. All statistical analyses were performed using SPSS software (SPSS software, v. 16.0; SPSS Inc., Chicago, IL). More details about these both procedures can be found in our previous publication [42].

3 Results

3.1 Occlusal contacts

Figure 2 displays both the bar graphs and the coloured mapping generated by the T-Scan, and those pressures computed by the FE simulation on the contact surfaces of each subject in both groups. The colour maps show the relative occlusal contact for each patient and the relative occlusion percentages on each hemiarch. In supplementary Table B.2, the numerical values of the mean, standard deviations, relative errors and asymmetrical index (AI) of both groups are summarized. Basically, a positive score of AI indicates superiority of the occlusal force on the right side, whereas a negative score indicates superiority on the left side. In all cases of the control group, the percentage difference between the measured occlusal contacts of both sides was below 12 %, with mean values (± SD) of 46.8 % and 53.2% (± 3.7) Whereas, in the UXB group, the difference between the pressures in both halves exceeds even 42% (S10), being always greater on the XS (mean value 62%) than on the NXS (mean value 38%). This imbalance produces a negative IA in all cases. Similar results were obtained by the FE approach, with also a greater percentage of occlusion on the XS (61%) than on the NXS (39%). As a result of the comparison between the numerical and experimental results, percent errors between both approaches were lower than 3.5 % for the control group and below 6 % for the UXB group. Furthermore, as can be seen in Figure 2, the occlusal pattern in both approaches was quite similar, with maximum values (red regions in Figure 2) on the same pairs of teeth. Meanwhile, the greatest differences occur in those contacts of low level (blue regions in Figure 2), resulting in almost negligible differences in the total occlusal percentages on both halves.

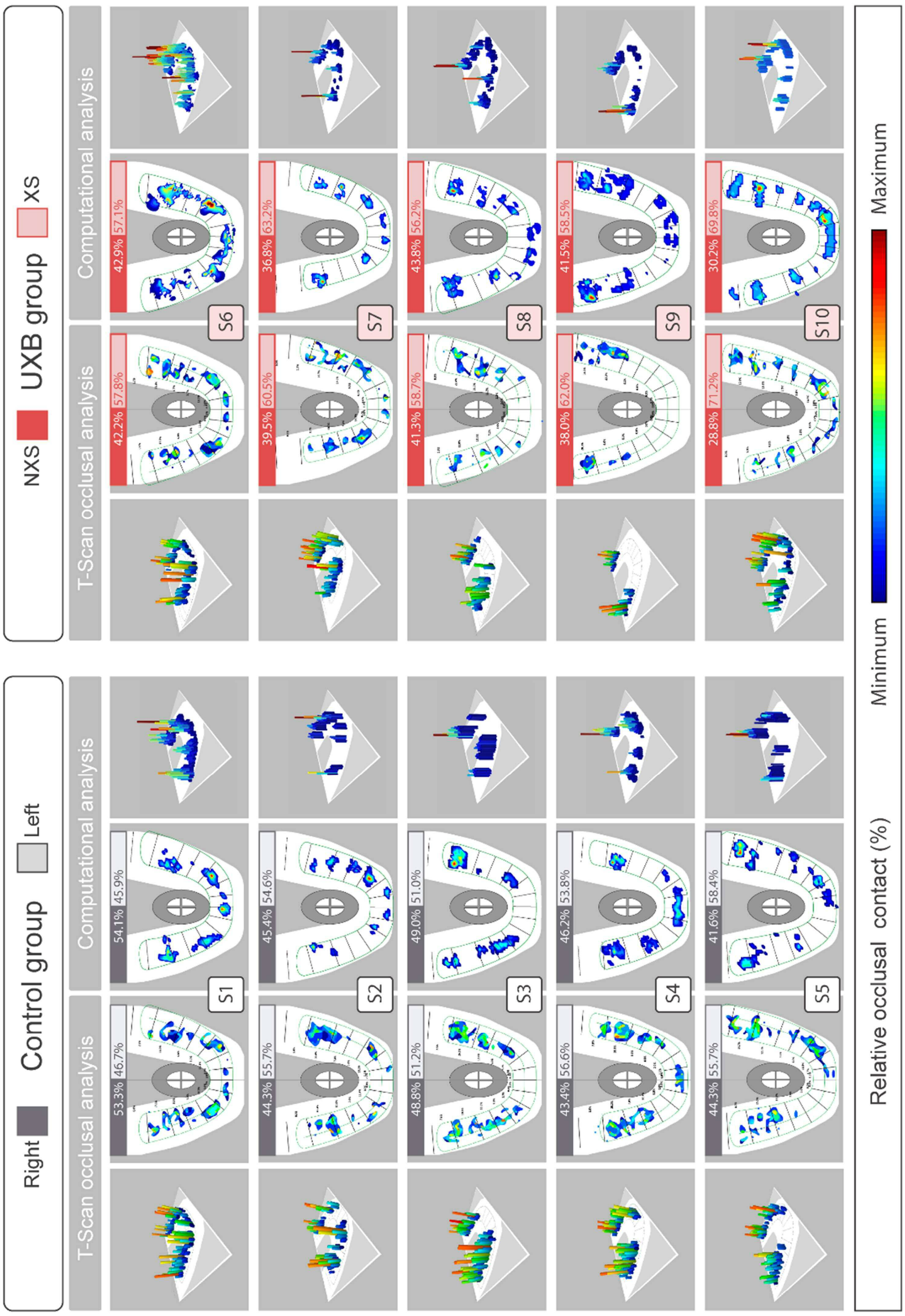

Figure 2. Perspective and top views of the occlusal records by the T-Scan III system and those computed through the FE analysis in each patient of the control group (left box) and the UXB group (right box).

3.2 Mechanical results

As was introduced, the occlusal forces subject PDLs to compressive stresses and strains, increasing, therefore, the hydrostatic pressure in the PDL's interstitial fluid. For many researchers [66–68], this increment is the main responsible of the tooth movement and bone remodelling process as it was first introduced by Schwarz in 1932 [69]. According to this "pressure-tension" theory, the overpressure could collapse the PDL's capillaries partially or completely, leading to a bone remodelling processes which may cause dental movement [68]. Physiologically, the range of capillary blood pressure has been stated to be within 2–4.7 kPa (15-35 mmHg) [70]. From this point of view, it is generally accepted [68] that bone remodelling occurs for values higher than 4.7 kPa of the volume-averaged hydrostatic pressure $\bar{\ }_H$. In our study, this variable was plotted for each PDL of the mandibular teeth in Figure 3, computing in each PDL element the $\bar{\ }_H$ as $\bar{\ }_H = (\sum_e \ {}^e_H \cdot \ {}^e)/\sum_e \ {}^e$ where ${}^e_H$ and ^{e} are respectively the hydrostatic pressure and the volume of an element, [68].

Hence, in the control group, the hydrostatic pressure was uniformly distributed along the PDLs of both halves, being greater in the posterior teeth than in the anterior ones. In those cases (i.e. see S2 in Figure 3) where the PDL's hydrostatic pressure overcame the maximum capillary blood pressure ($\bar{\ }^*_H =$ 4.7kPa) in one of the hemiarches, the hydrostatic reaction in the PDL of the other side was similar, potentially leading to symmetrical growth of both halves. Contrariwise, in the UXB group, the PDL's reactions were unbalanced in agreement with the occlusal analysis results, being always greater in the XS than in the NXS. In fact, in almost three of UXB subjects, $\bar{\ }_H$ exceeded the capillary blood in the XS. Finally, it is also noticeable that older subjects (S5 and S10) showed PDL's reactions in the second molar' ligaments due to the eruption of these teeth.

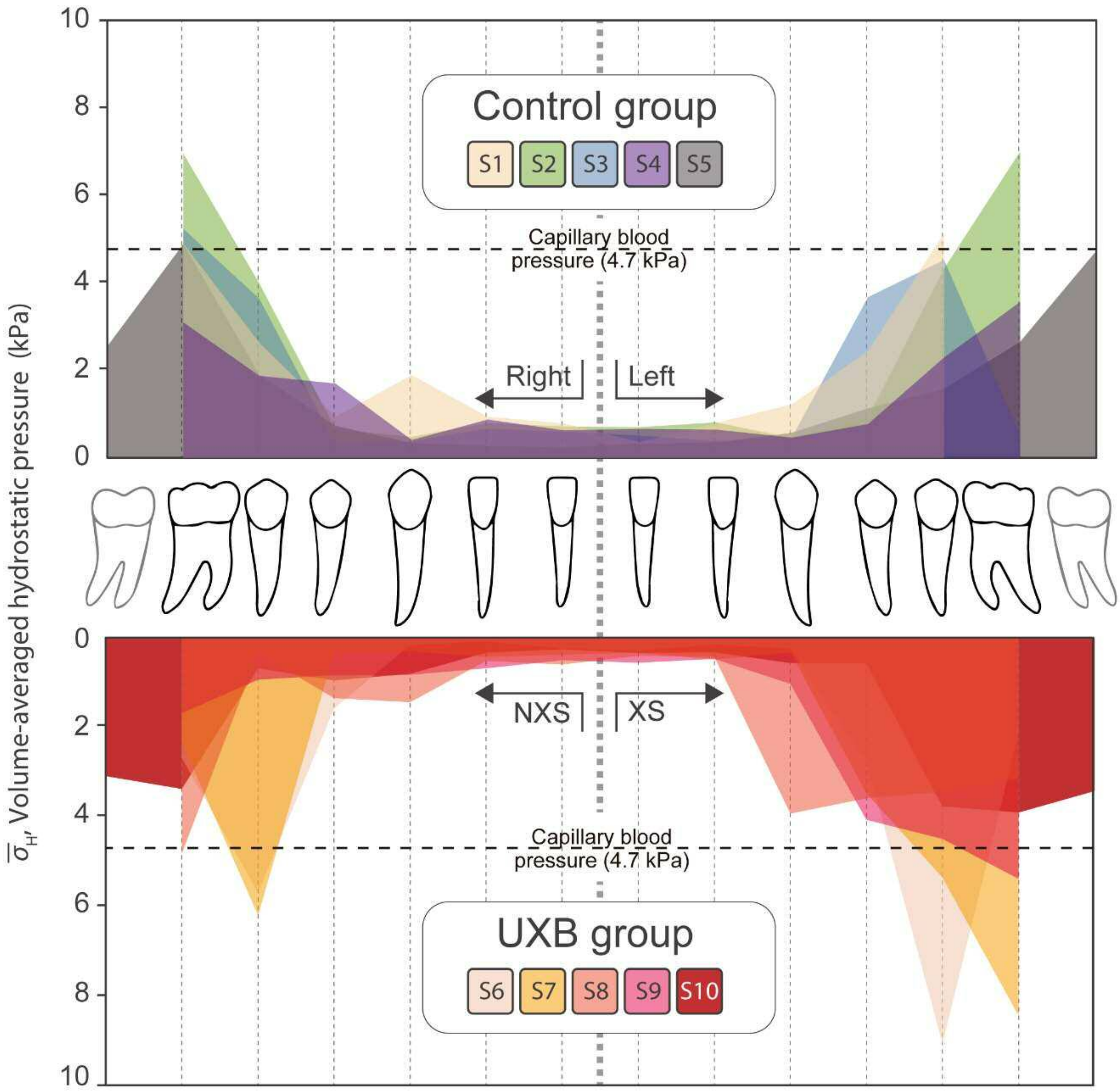

Figure 3. Volume-averaged hydrostatic pressure in each PDL of the inferior teeth of the patients of the Control (top) and UXB (bottom) groups. (For interpretation of the references to colour in this figure legend, the reader is referred to the web version of this article).

Likewise, based on the "pressure-tension" theory, the hydrostatic pressure of the cartilages could explain some of the morphological changes of the joint spaces and the condyle [26,27]. Hence, Figure 4 shows the difference in hydrostatic pressure between the two condylar cartilages, which is greater in the XS of UXB patients. As can be seen in Table 3, it is also notable that this pressure is higher in the condylar cartilage of the XS (1.16 ± 0.54 kPa) than in the one of the NXS side (0.78 ± 0.38 kPa).

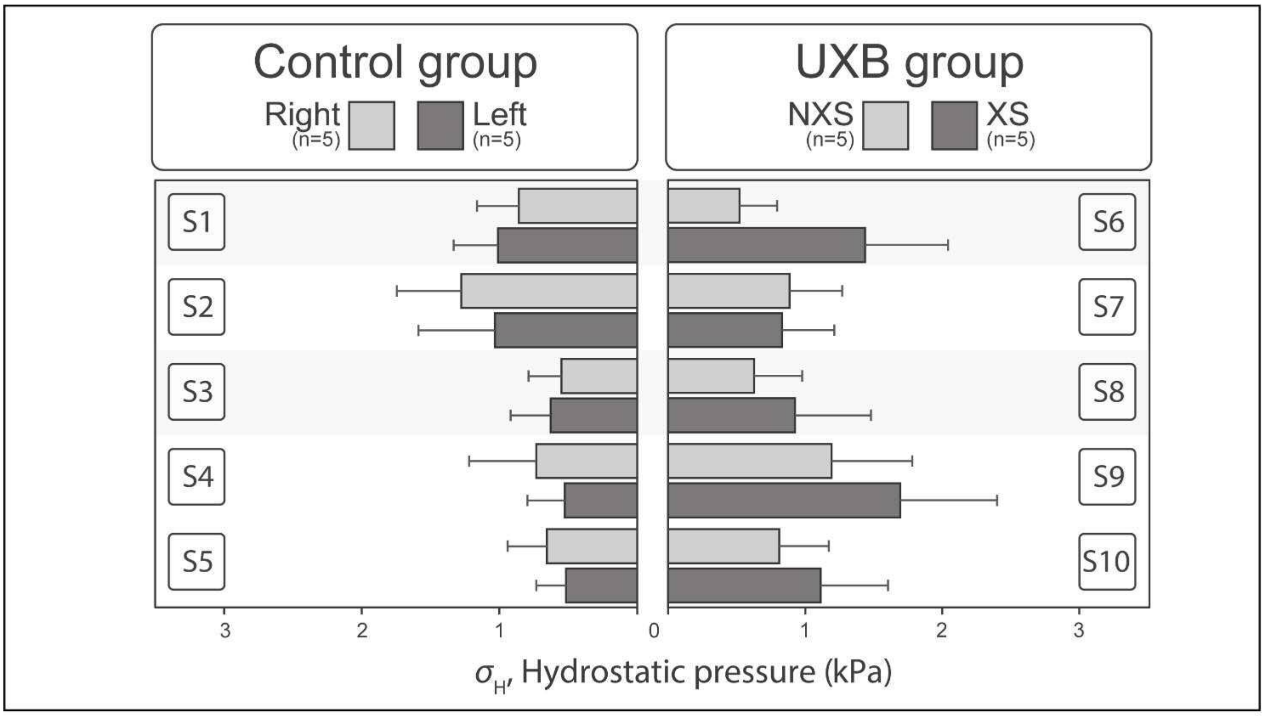

Figure. 4 Bar chart showing the mean value ± SD of the hydrostatic pressure in both condylar cartilages of the control and UXB groups.

Besides the pressure-tension theory [69], mandibular bone remodelling is often explained through the distortion or bending of the alveolar bone by the Frost mechanostat theory [71,72]. Regarding this, the minimum effective strain $_e$ is generally used as a measure of the overall tissue deformation gradient, being expressed from components of principal strains $(\ _1,\ \ _2,\ \ _3)$ by $\ _e = \sqrt{0.5 \cdot [(\ _1 - \ _2)^2 + (\ _2 - \ _3)^2 + (\ _3 - \ _1)^2]}$. During physiological activities, osteoblasts and osteoclasts work synchronously in a range between 0.0008 to 0.002-unit bone surface strain, which is often referred to lazy region. For $\ _e$ above this range, however, it is generally assumed that the bone volume could increase [72–74]. To evaluate the mandibular growth in our models according to this rule, the distribution of $\ _e$ in both mandibular halves of each model was shown in Figure 5. Red regions represented those areas in which bone apposition may occur following this mechanostat theory. As can be shown, higher strains were obtained at the coronoid processes and in the middle of the mandibular ramus as a result of the temporal and masseter muscle insertions respectively. Apart from these regions, it is also remarkable $_e$ values in the mandibular angle region, which are particularly pronounced on the XS side of the UXB patients. By contrast, in the control patients the $_e$ distribution was more balanced in both halves with maximum $_e$ values in both molar regions.

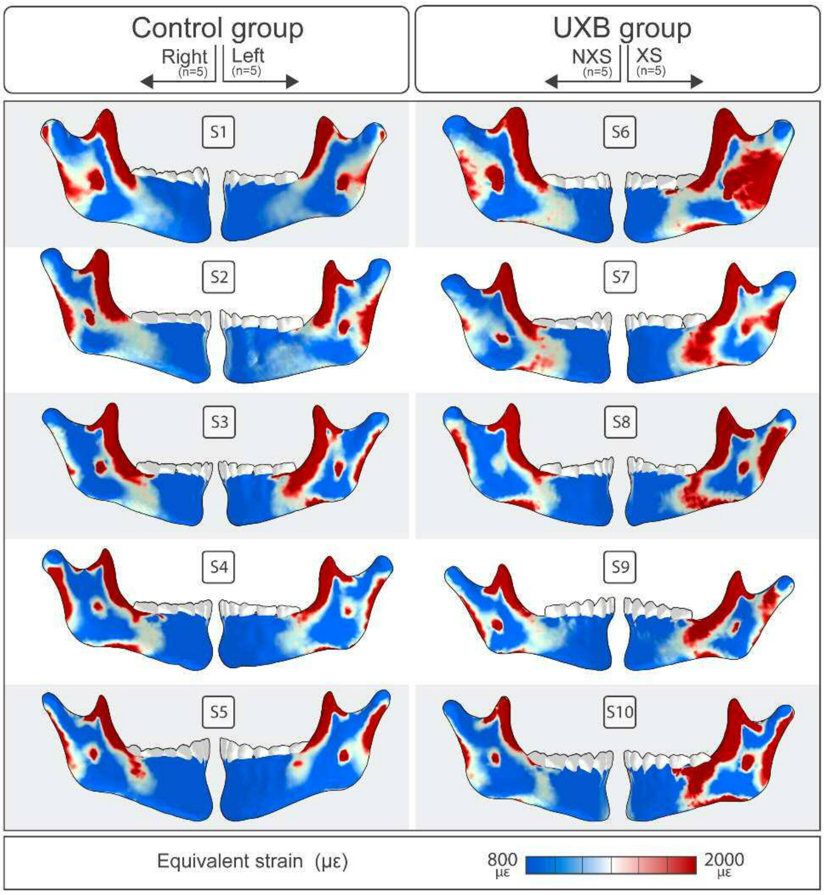

Figure 5. Distribution of the equivalent strain in both mandibular halves of those subjects of the control (left) and UXB groups (right).

In addition to the stress and strain results, the micro displacement patterns of the craniofacial structures were gathered from the FE analysis. Figure 6.A shows the lateral displacements of the maxilla (x-direction) while Figure 6.B shows its displacements in the anteroposterior direction (y-direction). Note that most control patients (S1, S4 and S5) show a symmetrical forward movement of the maxilla. The lateral displacement of each hemiarch was produced symmetrically towards a labial direction, potentially blending the maxilla around its sagittal midplane as part of a physiological expansion. In other cases (S2 and S3), maxilla's displacements were less pronounced and symmetric but always moves towards the anterior- labial direction. In UXB subjects, however, a non-symmetrical lateral displacement was observed, being mainly oriented towards the NXS. In fact, S7's maxilla experienced just the opposite movement that the observed in the control group, i.e. a displacement in labial direction. Likewise, the anterior displacement was neither symmetrical, being it greater on the NXS than on the opposite side. In the S9's maxilla, indeed, the hemiarch of the XS was posteriorly displaced.

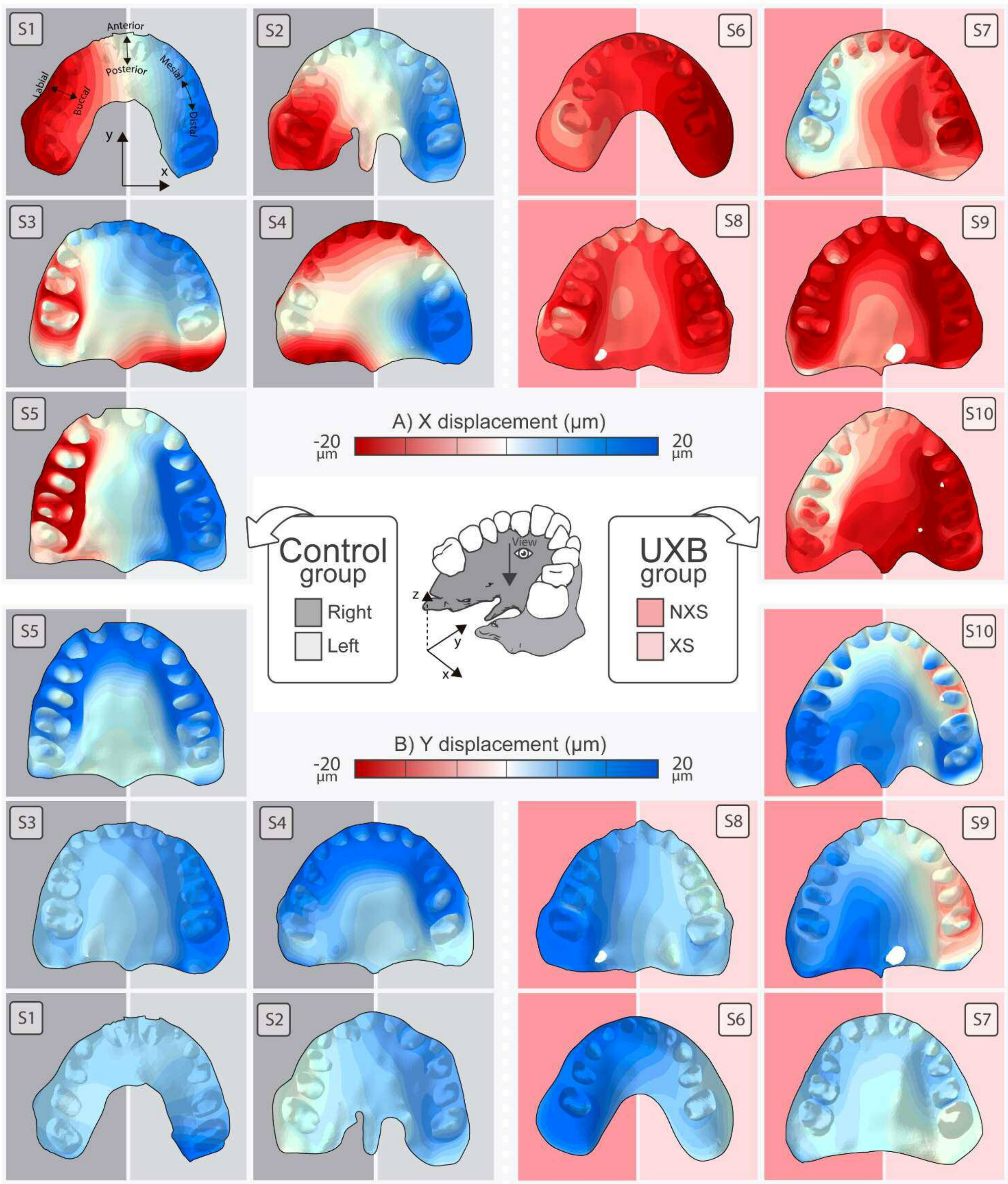

Figure 6. A) Lateral and B) anterior displacements of the maxilla in those subjects of the control (left) and UXB groups (right). Blue colour means positive displacement while red colour refers to negative displacements.

These differences were also noted on the upward displacement of craniofacial structures (shown in Figure 7). Whereas in control subjects, the occlusion moves the zygomatic and maxillary regions symmetrically and upward, in UXB subjects, this movement was just experimented by the XS' halve.

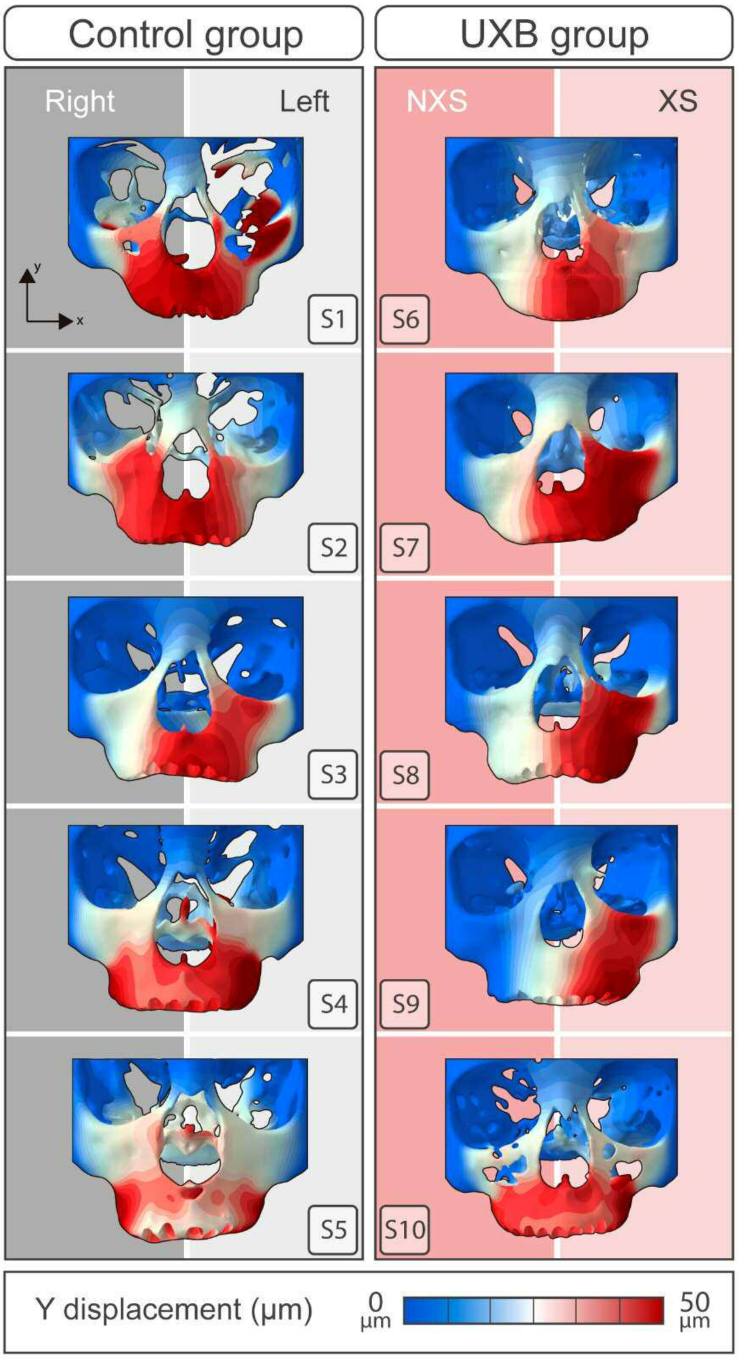

Figure 7. Coronal displacements of the skull in those subjects of the control (left) and UXB (right) groups. Red colour indicates upward movement, whereas blue colour denotes no displacement.

The above-mentioned mechanical results are summarised in Table 3. In the case of mandibular deformation and skull shift, the volume in mm3 with more than 2000 µε deformation or 50 µm displacement has been calculated respectively. Hence, it can be shown clearly that the crossbite presents a greater imbalance in the hydrostatic pressures of the soft tissues (PDLs and condylar cartilages), in the deformation of the mandible and the cranial misalignment, being in all of them, greater in the XS than in the contralateral side.

	Control group		*UXB group*	
	Right (n = 5)	Left (n = 5)	NXS (n = 5)	XS (n = 5)
Biomechanical measures	Mean ± SD	Mean ± SD	Mean ± SD	Mean ± SD
PDL hydrostatic pressure (kPa)	1.17 ± 1.76	1.10 ± 1.71	1.04 ± 1.71	2.50 ± 2.39
Condylar hydrostatic pressure (kPa)	0.78 ± 0.34	0.71 ± 0.32	0.78 ± 0.38	1.16 ± 0.54
Oclusal pressure (%)	47.3 ± 4.2	52.7 ± 4.2	39.0 ± 5.6	61.0 ± 5.6
Mandible volume with ε >2000 µε (mm^3)	2877 ± 325	3018 ± 409	2793 ±338	4111 ± 535
Skull volume displaced >50 µm (mm^3) in coronal direction	6994 ± 4850	8075± 3312	4388 ± 2209	11388 ± 1661

Table 3 Mean and standard deviation of the mechanical variables computed on both sides of the models from the control and UXB groups.

3.3 Morphological results

Finally, the normal distances between the surfaces of the original model and the mirrored one in each model of both groups were presented in Figure 8. From these results, as might be anticipated, the morphological difference between both halves was greater in UXB patients (out of ±3 mm range) than in the control subjects (within ± 2 mm range). A common aspect in all UXS patients was the backward position of the maxilla in the XS in comparison with its counterpart. This finding can also be observed in the average width of the maxilla (Table 4), being narrower for the hemimaxilla of the XS. Moreover, the mandible of these subjects was more forward on the XS side than on the NXS, except for S8 where just the contrary effect was obtained. This effect is caused because of the inherent definition of the crossbite, since the mandibular teeth occlude on the buccal side of the upper teeth, shifting the mandible to a more outward position on XS. The morphological variations between both sides were also noticeable in the temporal and zygomatic regions which were in a more posterior and upward position in the XS than in the NXS.

Figure 8. Normal distance between the original model and a mirrored model of the subjects of the control (left) and UXB (right) groups. Positive values (blue) means a forward position of this region against its counterpart, while negative values (red) indicate the backward position of the region.

Some of these morphological alterations were statistically quantified by Mann-Whitney analysis. Table 4 and Figure 9 show the mean values (± SD) of the computed bilateral measurements and their p-value signification. As can be seen, a significant difference was observed between the two sides in the width of the condyle, the length of the mandibular ramus, and the height of the maxillary region.

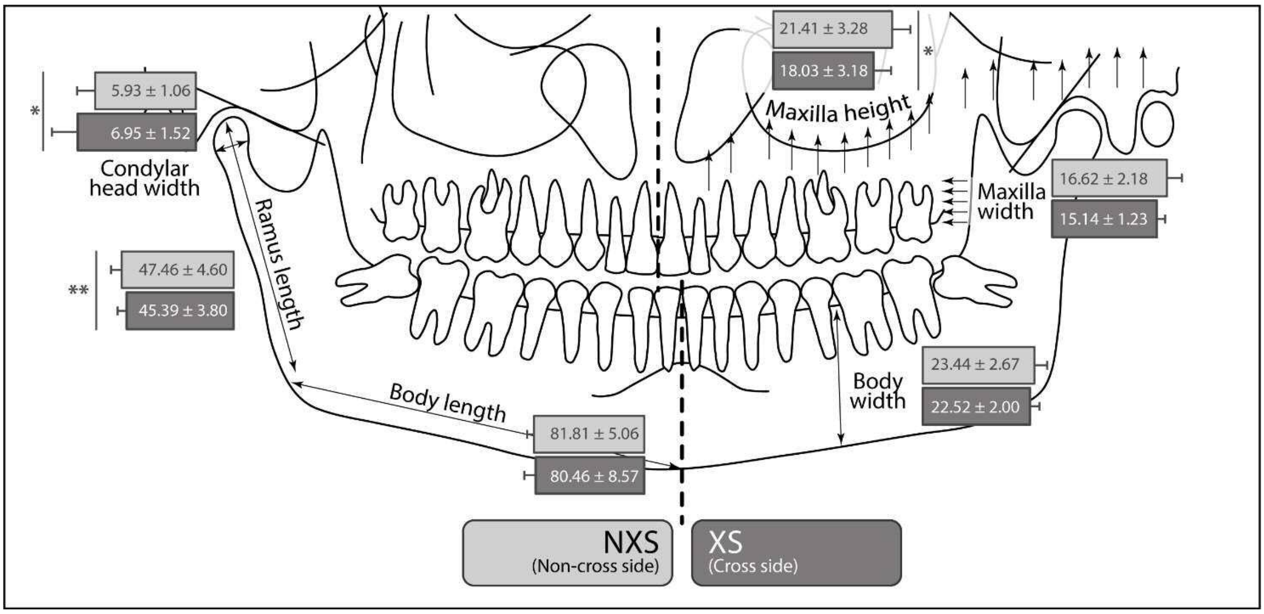

Figure. 9 Panoramic scheme of the morphological changes of the craniofacial complex in a patient with facial asymmetry. Bar chart showing the mean value ± SD of the measurements of the NXS (light grey) and XS (dark grey). Significant difference at $p < 0.05$ (*) and $p < 0.01$ (**).

	Control group			*UXB group*		
	Right (n = 5)	Left (n = 5)	Mann – Whitney	NXS (n = 5)	XS (n = 5)	Mann – Whitney
Bilateral measurements	Mean ± SD	Mean ± SD	p value	Mean ± SD	Mean ± SD	p value
Body length	79.91 ± 2.39	81.80 ± 3.48	0.4206	81.81 ± 5.06	80.46 ± 8.57	0.5442
Body width	21.87 ± 2.88	21.17 ± 1.12	0.8413	23.44 ± 2.67	22.52 ± 2.00	0.8474
Condylar head width	5.23 ± 0.84	6.01 ± 1.68	0.5476	5.93 ± 1.06	6.95 ± 1.52	0.0416*
Maxilla height	19.01 ± 1.66	20.65 ± 3.83	0.5476	21.41 ± 3.28	18.03 ± 3.18	0.0372*
Maxilla width	15.97 ± 1.73	17.29 ± 0.45	0.1508	16.62 ± 2.18	15.14 ± 1.23	0.0511
Ramus length	46.45 ± 2.90	48.44 ± 2.70	0.5476	47.46 ± 4.60	45.39 ± 3.80	0.0087**

Table 4 Comparison between the bilateral measurements of both sides in control and UXB groups. *Significant difference at $p < 0.05$ (*); $p < 0.01$ (**).

4 Discussion

As was previously introduced, many clinical [14,15] and computational [31,34–36] studies have attempted to understand the influence of the dental occlusion in the craniofacial development, and consequently, the influence of dental malocclusions in the craniofacial malformations. Nevertheless, the mechano-morphological relationship of craniofacial development during childhood is still uncertain [75].This uncertainty is mainly caused by the difficulty of evaluating biomechanically the craniofacial complex through the conventional experimental techniques [31] and because of the limitations of the computational methods, such as the developing of accurate FE models [37,38] of paediatric subjects. Fortunately, recent technological advances in 3D cephalometric images acquisition have allowed reducing the radiation for the patient in diagnosis, facilitating the craniofacial 3D modelling also in children. Moreover, the extended use of new devices for non-invasive occlusal analyses has encouraged checking the accuracy of these computational models. The aim of this study was, therefore, to demonstrate, the relationship between their craniofacial morphology with the occlusion, or rather between the asymmetrical morphology and the unilateral occlusion, through the development of complex and accurate FE models of paediatric subjects. Hence, the stress, strain and displacements computed from FE analyses at maximum intercuspation occlusion were compared with the asymmetrical morphology identified after a morphological 3D-analysis [42]. Although most of the population has a preferential chewing side, just in the most severe cases an unbalance in the occlusion occurs. Likewise, our occlusal analysis' outcomes (Figure 2) showed that the occlusal pattern in the control subjects was almost symmetrical with AI below 13.5 %. Consequently, it could be indicated that in these subjects the maximum intercuspation position coincides almost with the centric occlusion. According to the AI sign, however, our results suggest also that left side could be the referenced one in no pathological cases, in contrast with other studies [76–78] in which right side was found as preferential chewing side. This inconsistency with literature, however, could be explained by the modest size of our sample, in comparison with other clinical studies [76,77]. Furthermore, the low AI does not necessary mean an anomaly in the centred position of the occlusion [6] for these patients. On the contrary, in most UXB patients, the AI was greater than 20% and exceeds even 42% in S10, being in all cases the crossed side the one with the major occlusion. This result had been already observed by other clinical studies [79,80] which found that the occlusal contact is often shifted to the XS in patients with facial asymmetry. The occlusion patterns were also accurately simulated by our FE analyses, with an average relative error below 6%, which was close to the reliability errors of the T-Scan measurements [81]. These results prove, therefore, the truthfulness of our computational approach and its applicability to the goal of this study.

Besides the noticeable occlusal imbalance, UXB resulted also to an asymmetric distribution of the mechanical variables in the craniofacial complex, which could account some shape, size and position alterations that have been clinically observed previously [14,19,82]. In the case of the subjects of our study, these skeletal malformations were clearly highlighted through the 3D morphological and statistical analyses explained in section 3.3. Hence, apart from the specific variations of each subject, UXB patients displayed a common asymmetrical development on the mandible, maxilla and zygomatic region (shown in Figure 8). These variations, according to the FMH, could be explained by two different functional matrices: the periosteal and the capsular ones [83]. The first mainly modified the size and shape of the mandible, while the second altered the spatial position of the maxilla and cranial regions [84].

From the periosteal matrix perspective, our numerical results (shown in Figures 3 and 4) could explain some of the mandibular malformations founded in those subjects with UXB such as the more exterior position of the mandibular body, and the increase of the body and condyle width in the XS (shown in Figure 9 and Table 4). Hence, following the approach of other computational studies [67,85], we studied the periosteal functional matrix and condylar growth by the hydrostatic pressure (shown in Figure 3 and Figure 4) and the mandibular deformation (shown in Figure 5) following the principles of the pressure-tension [69] and Frost mechanostat [71,72] theories respectively. Applying them to our numerical results, bone remodelling and apposition patterns in the mandible could be described.

Hence, according to our results, the occlusion in those subjects with no UXB produced almost a symmetrical distribution of the hydrostatic pressure in the PDL's of both mandible's body halves. The symmetry was also found in those PDLs that exceeded the capillary blood pressure. According to the principles of the pressure-tension [69], this overpressure in both sides would lead to an almost symmetrical bone remodelling [68] of the mandible. Contrariwise, in the case of patients with UXB, an imbalance in the periodontal reaction was observed. Because of this imbalance, the hydrostatic pressure in several PDLs of the XS, mainly in the posterior PDLs, was higher than in those of the NXS, leading to a potentially overdevelopment of the mandible's XS side, as the observed in the morphological and statistical analysis (shown in Figure 9). Furthermore, as a result of periodontal overpressure, the bone remodelling around those teeth could occur, potentially leading to dental movements in the teeth of the XS [85]. This movement of XS' teeth would therefore aggravate and be responsible for UXB worsening over time. Thereby, our outcomes could serve as an analytical demonstration of the need of early treatments to correct malocclusions during childhood, as has already been empirically supported in several clinical studies [11,12,14,15].

On the other hand, the pressure imbalance was also noted in the condylar cartilages of UXB patients (Figure 4). According to the pressure-tension theory, this over-pressure in the XS's condyle (Table 3) could be behind the increase of the condylar thickness of the XS (shown in Figure 9). In paediatric patients, however, some studies [86,87] have not identified these morphological alterations early, since they may consolidate during adolescence [9,12].

Besides the effect of the periodontal stimulation on the development of the mandibular body, the principles of the Frost mechanostat theory [71,72] were also used to study the development of other mandibular regions, such as the mandibular branch or the posterior alveolar region. Results in Figure 5 display how centric occlusion leads to an almost-symmetric $_e$ distribution in the mandibles of non-UXB patients. Based on mechanostat theory principles, this balanced distribution leads to an almost symmetrical mandible's development. In addition to the symmetrical distribution of $_e$, it is noteworthy that $_e$ values above the upper limit of the lazy region (red regions in Figure 5) are only produced in those areas where the temporal and masseter muscles are inserted. Nevertheless, the strain state in these areas has not a useful meaning since it is caused by the concentration of local deformations on connector elements' attachments. By contrast, in UXB patients the $_e$ distribution was non-symmetric, which could lead to an asymmetrical development of the mandible, according to the mechanostat theory [71,72]. Besides, in all UXB's cases, it was also found that effective minimum strain in the molar and posterior regions of the mandibular half of the XS deformed is greater 0.002. This finding could provide an analytical proof of the periosteal matrix's' role in the craniofacial development and could supply an analytical evidence of a possible bone apposition in these regions, in agreement with previous clinical observations [19,20].

On the other hand, according to the FMH, the capsular matrix [84] of the mandible may be responsible for the asymmetry in the length of the mandibular ramus and body in patients with crossbite (see Table 4 and Figure 9). Based on the explanations of other authors [9,12], unilateral crossbite shifts the mandible towards the crossed side [16–18] producing a stretch of the mandibular structure of the contralateral side.

FMH is also responsible for the spatial transformations in the craniofacial regions, such as the more retracted and elevated position of the maxilla or zygomatic regions in the XS [83]. These spatial micro displacements, however, are difficult to measure experimentally because of their small size. Fortunately, computational approach, as the followed here, allowed us to identify the relative movements of these parts [82,88] through the nodes' displacements (shown in Figures 6 and 7). Therefore, it was found that the upper maxilla moved almost symmetrically along labial direction (shown in Figure 6.A) when the occlusion of non-UXB subjects was simulated. This movement could be interpreted according to its functional matrix as normal opening movement of it to the sagittal midplane [89]. In UXB patients, however, this movement was only followed by the NXS, whereas the counterpart moved towards the buccal direction (shown in Figure 6.A). In this case, the maxilla displacement could indicate just an inverse growth pattern, i.e. a narrowed development, as it was already noted in some clinical studies [21,90]. Likewise, this result was consistent with the displacement patterns and with the narrowing of its transverse dimension reported in our 3D morphological analysis (shown in Figure 8).

Regarding the anterior-posterior displacements of the maxilla (shown in Figure 6.B), it was found that non-UXB patients experienced a slight forward movement of the whole maxilla, while UXB patients experienced only the forward movement on the NXS. Indeed, in subjects S9 and S10, there was even a backward movement of the half maxilla of XS, which could represent the maxilla rotation around the sagittal axis, as had been previously reported [90].

As a consequence of the reaction of upper teeth, the occlusion causes the upward movement of the maxilla and consequently of the adjacent zygomatic region (shown in Figure 7). In non-UXB patients, this upward movement was practically symmetrical throughout the whole maxilla (see red regions in Figure 7). Nevertheless, in those patients with UXB, the unilateral occlusion caused just this effect in the XS (shown in Figure 7). This result is in agreement with recent clinical findings [91], which have found a significant elevation of the zygomatic region of the XS in patients with UXB. This finding was also consistent with the results of our 3D morphological analysis (see Figure 8), which displayed a clear asymmetry in the maxillary-zygomatic regions possibly caused by the upward movement of these regions at the unilateral occlusion. In some cases, such as S6 and S7 ones, the spatial asymmetry was even extended to the temporal region of the skull, which could additionally be influenced by the functional asymmetry of the chewing muscles. From our results, therefore, it is possible to establish a relationship between the craniofacial structures' movements with their spatial positioning, in agreement with their capsule matrixes.

This computational approach is, therefore, an important step in the study of FMH by computational models since it allows relating the mechanical stimulation of unilateral occlusion with the craniofacial development in children with UXB. Furthermore, up to now, this study presents the widest sample of craniofacial complex's FE models of children to study the FMH. It is also remarkable that the mechanical properties, muscular forces and modelling techniques here summarized could be a good reference for future engineers, researchers and clinical experts in the modelling of the paediatric craniofacial complex.

4.1 Study limitations

This study presents, however, several limitations that must be considered for the interpretation of the results and that future studies should address. Firstly, as is common in computational studies [40,41], the sample size was smaller than those used in clinical studies of the literature [15,16,19]. This limitation is mainly due to the computational models requiring much more post-processing of the images than the one needed for clinical studies. In addition, the complexity of the shapes and the many contacts involved in the craniofacial complex complicate the modelling and convergence of computational models, in comparison to others with simpler geometries such as the femur [92,93]. On the hand, the sample was not homogeneous and involved individuals of different ages (6-12 years old) and both sexes, which may have led to mixed results. Although the craniofacial growth differences in both genders have not been considered statistically significant at ages before puberty[94,95], a uniform scaling of the sample was carried out (shown in section 2.1). In our work, the sample size was mainly conditioned by the difficulties of obtaining CBCT images in paediatric patient, such as the radiation exposure, the scanning time or the natural nervousness of children. Despite the challenge of doing CBCT scans, our findings have demonstrated their potential in the assessment of the UXB, encouraging to further researchers to perform larger databases that improve the understanding of the effect of UXB on the craniofacial development. We believe that a wider sample with equal gender distribution could result in more reliable and precise results, allowing even the study of shape variability of patients with facial asymmetry through Statistical Shape Models (SSMs).

Regarding the modelling procedure, the use of intraoral scanners and magnetic resonance imaging (MRI) images could improve respectively the geometrical definition of the occlusal plane and the soft tissues. Due to this limitation and the lack of data for paediatric patients, the articular discs, for instance, were defined based on the free space between the fibrocartilage layers, which could be leading to deviations from the real disc geometry. Likewise, for some tissues such as the periodontal ligament or the articular surfaces of cartilages, uniform thickness was assumed, which could differ from reality. In the case of condylar cartilage, for instance, it was considered a thickness agreed with some studies of the literature [44,52], but lower than the one used in other [96,97]. MRI imaging may also provide useful additional insights about the changes caused by UXB in the size and length of the muscles on both sides, or in the relation between the condyle and the articular disc. Moreover, it is important also to consider the challenge of performing these procedures in children without sedation. Likewise, a not superficial electromyography (EMG) study of the muscle activation in each patient would allow a more precise definition of the muscular activity, which is particularly important for defining the functional asymmetry in patients with UXB. Notwithstanding this, non-superficial EMGs are misadvised for the study of muscular activations in childhood because of the potential risks and implications for the child. Moreover, avoiding the challenge of treating children, other experimental tests such as in vivo occlusal analysis would yield more reliable occlusion patterns than those obtained using 3D printed pieces. The occlusal analyses could also be improved quantifying the specific reaction on each tooth, which could contribute to validate the computational models more precisely. Finally, our results suggested some possible morphological alterations based on the mechanical reactions in some tissues, but without applying any bone remodelling algorithm. We consider that current bone remodelling algorithms [85,98] should be carefully applied to the craniofacial complex since its development is conditioned by several interrelated factors such as the teeth eruption, the hormonal growth, the diet's consistency, breathing habits, amongst others. Notwithstanding all these limitations, this study is a first step in the understanding of the occlusion's effect on children's craniofacial development following the FMH principles. Future studies should address genetic and hormonal factors, or other functions effects on craniofacial development to describe then bone remodelling algorithms that integrate all these aspects.

5 Conclusion

This study computationally relates the biomechanical outcomes caused by unilateral occlusion with the morphological variations detected in paediatric patients with UXB according to the FMH's principles, leading the following conclusions:

- FE analysis is an effective tool for the biomechanical evaluation of unilateral crossbite, mimicking faithfully the occlusal patterns with a mean error below 6 %.
- Patients with unilateral crossbite showed a functional imbalance of up to 42% at both occlusal and periodontal levels.
- The interstitial fluid overpressure (> 4.7 kPa) in the periodontium of the crossed side could be responsible for the malocclusion worsening over time, based on the pressure-tension theory. It is

crucial, therefore, to perform early treatments that compensate for the mechanical stimulation of the periodontium in both hemiarches.

- Mandibular over deformation ($>2000\ \varepsilon$) could explain the thickening of the molar region in the crossed side’s mandibular body.
- Periodontal overpressure and mandibular over deformation are great predictors of asymmetric mandibular development in paediatric patients with unilateral crossbite, being consistent with the periosteal matrix principles of the FMH.
- Maxilla and zygomatic region movements reproduce the misplacement of these structures in patients with unilateral crossbite, in agreement with their capsular matrices.
- FE analysis is an effective tool for evaluating the effect of periosteal and capsular matrices on the craniofacial development, supporting the FMH’s principles.

Conflict of interests

The authors declare that the research was conducted in the absence of any commercial or financial relationships that could be construed as a potential conflict of interest.

Author Contributions

Javier Ortún-Terrazas: Data curation (CAE Preprocessing); Investigation; Methodology; Formal analysis; Software; Visualization; Writing - Original Draft.

Michael J. Fagan: Methodology; Formal analysis; Supervisor; Writing - Original Draft.

José Cegoñino: Project administration; Resources; Validation; Software; Visualization; Writing - Review & Editing.

Edson Illipronti-Filho: Data curation (Segmentation); Investigation; Resources; Visualization.

Amaya Perez del Palomar: Conceptualization; Validation; Funding acquisition; Project administration; Supervisor; Writing - Review & Editing.

Funding

This work was supported by the Spanish Ministry of Economy and Competitiveness (project DPI 2016-79302-R), the European Social Funds and Regional Government of Aragon (grant 2016/20) and Ibercaja-Cai Foundation (grant IT 4/18).

Acknowledgements

The authors would like to thank Dr. Ángel Sampietro Fuentes for his assistance in this research

References

[1] D.M. Ranly, Craniofacial growth., Dental Clinics of North America. 44 (2000) 457–70, v.

[2] G. Castaldo, F. Cerritelli, Craniofacial growth: evolving paradigms, CRANIO®. 33 (2015) 23–31. https://doi.org/10.1179/0886963414Z.00000000042.

[3] M.L. Moss, R.M. Rankow, The role of the functional matrix in mandibular growth, The Angle Orthodontist. 38 (1968) 95–103.

[4] M.L. Moss, The role of muscular functional matrices in development and maintenance of occlusion., Bulletin - Pacific Coast Society of Orthodontists. 45 (1970) 29–30.

[5] L.C. Hodge, P.E. Mahan, A study of mandibular movement from centric occlusion to maximum intercuspation, The Journal of Prosthetic Dentistry. 18 (1967) 19–30. https://doi.org/10.1016/0022-3913(67)90107-2.

[6] J. Martinez-Gomis, M. Lujan-Climent, S. Palau, J. Bizar, J. Salsench, M. Peraire, Relationship between chewing side preference and handedness and lateral asymmetry of peripheral factors, Archives of Oral Biology. 54 (2009) 101–107. https://doi.org/10.1016/j.archoralbio.2008.09.006.

[7] B. Thilandera, Orthodontic relapse versus natural development, American Journal of Orthodontics and Dentofacial Orthopedics. 117 (2000) 562–563. https://doi.org/10.1016/S0889-5406(00)70200-9.

[8] B. Thilander, B. Lennartsson, A Study of Children with Unilateral Posterior Crossbite, Treated and Untreated, in the Deciduous Dentition, Journal of Orofacial Orthopedics / Fortschritte Der Kieferorthopädie. 63 (2002) 371–383. https://doi.org/10.1007/s00056-002-0210-6.

[9] M.G. Piancino, S. Kyrkanides, Understanding Masticatory Function in Unilateral Crossbites, John Wiley & Sons, Inc., Oxford, UK, 2016. https://doi.org/10.1002/9781118971901.

[10] A. Björk, A.A. Krebs, B. Solow, A Method for Epidemiological Registration of Malocculusion, Acta Odontologica Scandinavica. 22 (1964) 27–41.

[11] M. Malandris, E.K. Mahoney, Aetiology, diagnosis and treatment of posterior cross-bites in the primary dentition, International Journal of Paediatric Dentistry. 14 (2004) 155–166.

[12] P. Planas, Neuro-occlusal rehabilitation: NOR, 2nd ed., Amolca, Barcelona, España, 2013.

[13] S. Petrén, L. Bondemark, B. Söderfeldt, A systematic review concerning early orthodontic treatment of unilateral posterior crossbite, The Angle Orthodontist. 73 (2003) 588–596.

[14] D.B. Kennedy, M. Osepchook, Unilateral posterior crossbite with mandibular shift: a review, Journal-Canadian Dental Association. 71 (2005) 569.

[15] P. Agostino, A. Ugolini, A. Signori, A. Silvestrini-Biavati, J.E. Harrison, P. Riley, Orthodontic treatment for posterior crossbites, Cochrane Database of Systematic Reviews. (2014).

[16] K. Ishizaki, K. Suzuki, T. Mito, E.M. Tanaka, S. Sato, Morphologic, functional, and occlusal characterization of mandibular lateral displacement malocclusion, American Journal of Orthodontics and Dentofacial Orthopedics. 137 (2010) 454-e1.

[17] J. Primožič, M. Ovsenik, S. Richmond, C.H. Kau, A. Zhurov, Early crossbite correction: a three-dimensional evaluation, The European Journal of Orthodontics. 31 (2009) 352–356.

[18] T. Gazit-Rappaport, M. Weinreb, E. Gazit, Quantitative evaluation of lip symmetry in functional asymmetry, The European Journal of Orthodontics. 25 (2003) 443–450.

[19] Veli, T. Uysal, T. Ozer, F.I. Ucar, M. Eruz, Mandibular asymmetry in unilateral and bilateral posterior crossbite patients using cone-beam computed tomography, The Angle Orthodontist. 81 (2011) 966–974. https://doi.org/10.2319/022011-122.1.

[20] G.O. Ramirez-Yanez, A. Stewart, E. Franken, K. Campos, Prevalence of mandibular asymmetries in growing patients, The European Journal of Orthodontics. 33 (2011) 236–242. https://doi.org/10.1093/ejo/cjq057.

[21] S. Melink, M.V. Vagner, I. Hocevar-Boltezar, M. Ovsenik, Posterior crossbite in the deciduous dentition period, its relation with sucking habits, irregular orofacial functions, and otolaryngological findings, American Journal of Orthodontics and Dentofacial Orthopedics. 138 (2010) 32–40. https://doi.org/10.1016/j.ajodo.2008.09.029.

[22] E. Defraia, A. Marinelli, G. Baroni, I. Tollaro, Dentoskeletal effects of a removable appliance for expansion of the maxillary arch: a postero-anterior cephalometric study, The European Journal of Orthodontics. 30 (2007) 57–60.

[23] B.J. Langberg, K. Arai, R.M. Miner, Transverse skeletal and dental asymmetry in adults with unilateral lingual posterior crossbite, American Journal of Orthodontics and Dentofacial Orthopedics. 127 (2005) 6–15. https://doi.org/10.1016/j.ajodo.2003.10.044.

[24] J.-Y. Kim, H.-D. Jung, Y.-S. Jung, C.-J. Hwang, H.-S. Park, A simple classification of facial asymmetry by TML system., Journal of Cranio-Maxillo-Facial Surgery : Official Publication

of the European Association for Cranio-Maxillo-Facial Surgery. 42 (2014) 313–20. https://doi.org/10.1016/j.jcms.2013.05.019.

[25] A.R. Sepahdari, S. Mong, Skull base CT: normative values for size and symmetry of the facial nerve canal, foramen ovale, pterygoid canal, and foramen rotundum., Surgical and Radiologic Anatomy : SRA. 35 (2013) 19–24. https://doi.org/10.1007/s00276-012-1001-4.

[26] E. Miyatake, S. Miyawaki, Y. Morishige, A. Nishiyama, A. Sasaki, T. Takano-Yamamoto, Class III malocclusion with severe facial asymmetry, unilateral posterior crossbite, and temporomandibular disorders, American Journal of Orthodontics and Dentofacial Orthopedics. 124 (2003) 435–445. https://doi.org/10.1016/S0889-5406(03)00562-6.

[27] B.S. Almaqrami, M.S. Alhammadi, B. Tang, E.S. ALyafrusee, F. Hua, H. He, Three-dimensional morphological and positional analysis of the temporomandibular joint in adults with posterior crossbite: A cross-sectional comparative study, Journal of Oral Rehabilitation. 48 (2021) 666–677. https://doi.org/10.1111/joor.13156.

[28] K.L. Hesse, J. Årtun, D.R. Joondeph, D.B. Kennedy, Changes in condylar position and occlusion associated with maxillary expansion for correction of functional unilateral posterior crossbite, American Journal of Orthodontics and Dentofacial Orthopedics. 111 (1997) 410–418. https://doi.org/10.1016/S0889-5406(97)80023-6.

[29] M.-Q. Wang, J.-J. He, G. Li, S.E. Widmalm, The effect of physiological nonbalanced occlusion on the thickness of the temporomandibular joint disc: A pilot autopsy study, The Journal of Prosthetic Dentistry. 99 (2008) 148–152. https://doi.org/10.1016/S0022-3913(08)60031-1.

[30] D.R. Myers, J.T. Barenie, R.A. Bell, E.H. Williamson, Condylar position in children with functional posterior crossbites: before and after crossbite correction., Pediatric Dentistry. 2 (1980) 190–4.

[31] P. O'Higgins, L.C. Fitton, R. Phillips, J. Shi, J. Liu, F. Gröning, S.N. Cobb, M.J. Fagan, Virtual Functional Morphology: Novel Approaches to the Study of Craniofacial Form and Function, Evolutionary Biology. 39 (2012) 521–535. https://doi.org/10.1007/s11692-012-9173-8.

[32] T. Kofod, P.M. Cattaneo, M. Dalstra, B. Melsen, Three-Dimensional Finite Element Analysis of the Mandible and Temporomandibular Joint During Vertical Ramus Elongation by Distraction Osteogenesis, Journal of Craniofacial Surgery. 16 (2005) 586–593. https://doi.org/10.1097/01.SCS.0000157305.60505.B5.

[33] P.M. Cattaneo, T. Kofod, M. Dalstra, B. Melsen, Using the finite element method to model the biomechanics of the asymmetric mandible before, during and after skeletal correction by distraction osteogenesis., Computer Methods in Biomechanics and Biomedical Engineering. 8 (2005) 157–65. https://doi.org/10.1080/10255840512331388731.

[34] J.H.H. Koolstra, T.M.G.J.M.G.J. van Eijden, Combined finite-element and rigid-body analysis of human jaw joint dynamics, Journal of Biomechanics. 38 (2005) 2431–2439. https://doi.org/10.1016/j.jbiomech.2004.10.014.

[35] J. Libby, A. Marghoub, D. Johnson, R.H. Khonsari, M.J. Fagan, M. Moazen, Modelling human skull growth: a validated computational model, Journal of The Royal Society Interface. 14 (2017) 20170202. https://doi.org/10.1098/rsif.2017.0202.

[36] A. Marghoub, J. Libby, C. Babbs, E. Pauws, M.J. Fagan, M. Moazen, Predicting calvarial growth in normal and craniosynostotic mice using a computational approach, Journal of Anatomy. 10 (2017) 440–448. https://doi.org/10.1111/joa.12764.

[37] P.S. Donzelli, L.M. Gallo, R.L. Spilker, S. Palla, Biphasic finite element simulation of the TMJ disc from in vivo kinematic and geometric measurements., Journal of Biomechanics. 37 (2004) 1787–91. https://doi.org/10.1016/j.jbiomech.2004.01.029.

[38] S. Benazzi, H.N. Nguyen, O. Kullmer, K. Kupczik, Dynamic modelling of tooth deformation using occlusal kinematics and finite element analysis, PLoS ONE. 11 (2016) 1–17. https://doi.org/10.1371/journal.pone.0152663.

[39] D.-S. Choi, B.-K. Cha, I. Jang, K.-H. Kang, S.-C. Kim, Three-dimensional finite element analysis of occlusal stress distribution in the human skull with premolar extraction, The Angle Orthodontist. 83 (2013) 204–211. https://doi.org/10.2319/020112-89.1.

[40] S. Sana, R.T. Kondody, A.K. Talapaneni, A. Fatima, S.L. Bangi, Occlusal stress distribution in the human skull with permanent maxillary first molar extraction: A 3-dimensional finite element study, American Journal of Orthodontics and Dentofacial Orthopedics. 160 (2021) 552–559. https://doi.org/10.1016/j.ajodo.2020.05.022.

[41] P.G.M. Knoops, A. Borghi, F. Ruggiero, G. Badiali, A. Bianchi, C. Marchetti, N. Rodriguez-Florez, R.W.F. Breakey, O. Jeelani, D.J. Dunaway, S. Schievano, A novel soft tissue prediction methodology for orthognathic surgery based on probabilistic finite element modelling, PLOS ONE. 13 (2018) e0197209. https://doi.org/10.1371/journal.pone.0197209.

[42] J. Ortún-Terrazas, M.J. Fagan, J. Cegoñino, E. Illipronti-Filho, A. Pérez del Palomar, Towards an early 3D-diagnosis of craniofacial asymmetry by computing the accurate midplane: A PCA-based method, Computer Methods and Programs in Biomedicine. 191 (2020) 105397. https://doi.org/10.1016/j.cmpb.2020.105397.

[43] A.G.A.A.G. Pullinger, F. Baldioceda, C.A.C.A. Bibb, Relationship of TMJ Articular Soft Tissue to Underlying Bone in Young Adult Condyles, Journal of Dental Research. 69 (1990) 1512–1518. https://doi.org/10.1177/00220345900690081301.

[44] H. Mori, S. Horiuchi, S. Nishimura, H. Nikawa, T. Murayama, K. Ueda, D. Ogawa, S. Kuroda, F. Kawano, H. Naito, M. Tanaka, J.H. Koolstra, E. Tanaka, Three-dimensional finite element analysis of cartilaginous tissues in human temporomandibular joint during prolonged clenching., Archives of Oral Biology. 55 (2010) 879–86. https://doi.org/10.1016/j.archoralbio.2010.07.011.

[45] T. Hansson, B. Nordström, Thickness of the soft tissue layers and articular disk in temporomandibular joints with deviations in form, Acta Odontologica Scandinavica. 35 (1977) 281–288. https://doi.org/10.3109/00016357709064126.

[46] G. Pietrzak, A. Curnier, J. Botsis, S. Scherrer, A. Wiskott, U. Belser, A nonlinear elastic model of the periodontal ligament and its numerical calibration for the study of tooth mobility., Computer Methods in Biomechanics and Biomedical Engineering. 5 (2002) 91–100. https://doi.org/10.1080/10255840290032117.

[47] L. Keilig, M. Drolshagen, K.L. Tran, I. Hasan, S. Reimann, J. Deschner, K.T. Brinkmann, R. Krause, M. Favino, C. Bourauel, In vivo measurements and numerical analysis of the biomechanical characteristics of the human periodontal ligament, Annals of Anatomy - Anatomischer Anzeiger. 206 (2016) 80–88. https://doi.org/10.1016/j.aanat.2015.08.004.

[48] B. Xu, Y. Wang, Q. Li, Modeling of damage driven fracture failure of fiber post-restored teeth, Journal of the Mechanical Behavior of Biomedical Materials. 49 (2015) 277–289. https://doi.org/10.1016/j.jmbbm.2015.05.006.

[49] J. Ortún-Terrazas, J. Cegoñino, U. Santana-Penín, U. Santana-Mora, A. Pérez del Palomar, Approach towards the porous fibrous structure of the periodontal ligament using micro-computerized tomography and finite element analysis, Journal of the Mechanical Behavior of Biomedical Materials. 79 (2018) 135–149. https://doi.org/10.1016/j.jmbbm.2017.12.022.

[50] S. Ingawalé, T. Goswami, Temporomandibular Joint: Disorders, Treatments, and Biomechanics, Annals of Biomedical Engineering. 37 (2009) 976–996. https://doi.org/10.1007/s10439-009-9659-4.

[51] L. Ruggiero, B.K. Zimmerman, M. Park, L. Han, L. Wang, D.L. Burris, X.L. Lu, Roles of the Fibrous Superficial Zone in the Mechanical Behavior of TMJ Condylar Cartilage, Annals of Biomedical Engineering. 43 (2015) 2652–2662. https://doi.org/10.1007/s10439-015-1320-9.

[52] M. Singh, M.S. Detamore, Tensile properties of the mandibular condylar cartilage., Journal of Biomechanical Engineering. 130 (2008) 011009. https://doi.org/10.1115/1.2838062.

[53] G. Holzapfel, Nonlinear Solid Mechanics: A Continuum Approach for Engineering, Wiley, New York. (2000).

[54] B. Storakers, On material representation and constitutive branching in finite compressible elasticity, Journal of the Mechanics and Physics of Solids. 34 (1986) 125–145. https://doi.org/10.1016/0022-5096(86)90033-5.

[55] M. Argoubi, A. Shirazi-Adl, Poroelastic creep response analysis of a lumbar motion segment in compression, Journal of Biomechanics. 29 (1996) 1331–1339. https://doi.org/10.1016/0021-9290(96)00035-8.

[56] M. Bergomi, J. Cugnoni, M. Galli, J. Botsis, U.C. Belser, H.W.A. Wiskott, Hydro-mechanical coupling in the periodontal ligament: A porohyperelastic finite element model, Journal of Biomechanics. 44 (2011) 34–38. https://doi.org/10.1016/j.jbiomech.2010.08.019.

[57] G. Frongia, G. Ramieri, C. de Biase, P. Bracco, M.G. Piancino, Changes in electric activity of masseter and anterior temporalis muscles before and after orthognathic surgery in skeletal class III patients, Oral Surgery, Oral Medicine, Oral Pathology and Oral Radiology. 116 (2013) 398–401. https://doi.org/10.1016/j.oooo.2013.06.008.

[58] C. Martín, J.C. Palma, J.M. Alamán, J.M. Lopez-Quiñones, J.A. Alarcón, Longitudinal evaluation of sEMG of masticatory muscles and kinematics of mandible changes in children treated for unilateral cross-bite, Journal of Electromyography and Kinesiology. 22 (2012) 620–628. https://doi.org/10.1016/j.jelekin.2012.01.002.

[59] J. Ortún-Terrazas, J. Cegoñino, A. Pérez del Palomar, In silico study of cuspid' periodontal ligament damage under parafunctional and traumatic conditions of whole-mouth occlusions. A patient-specific evaluation, Computer Methods and Programs in Biomedicine. 184 (2020) 105107. https://doi.org/10.1016/j.cmpb.2019.105107.

[60] D. Lacroix, P.J. Prendergast, A mechano-regulation model for tissue differentiation during fracture healing: analysis of gap size and loading, Journal of Biomechanics. 35 (2002) 1163–1171. https://doi.org/10.1016/S0021-9290(02)00086-6.

[61] J. Ortún-Terrazas, J. Cegoñino, U. Santana-Penín, U. Santana-Mora, A. Pérez del Palomar, Computational analysis of craniomandibular tissues for the correction of mandibular asymmetries in childhood, 23rd Congress of the European Society of Biomechanics. (2017). https://doi.org/10.5281/zenodo.3775321.

[62] J.W. DeVocht, V.K. Goel, D.L. Zeitler, D. Lew, A study of the control of disc movement within the temporomandibular joint using the finite element technique, Journal of Oral and Maxillofacial Surgery. 54 (1996) 1431–1437. https://doi.org/10.1016/S0278-2391(96)90259-1.

[63] J. Zheng, Z.R. Zhou, J. Zhang, H. Li, H.Y. Yu, On the friction and wear behaviour of human tooth enamel and dentin, Wear. 255 (2003) 967–974. https://doi.org/10.1016/S0043-1648(03)00079-6.

[64] E. Tanaka, N. Kawai, M. Tanaka, M. Todoh, T. van Eijden, K. Hanaoka, D.A. Dalla-Bona, T. Takata, K. Tanne, The Frictional Coefficient of the Temporomandibular Joint and Its Dependency on the Magnitude and Duration of Joint Loading, Journal of Dental Research. 83 (2004) 404–407. https://doi.org/10.1177/154405910408300510.

[65] M. Pinheiro, X. Ma, M.J. Fagan, G.T. McIntyre, P. Lin, G. Sivamurthy, P.A. Mossey, A 3D cephalometric protocol for the accurate quantification of the craniofacial symmetry and facial growth, Journal of Biological Engineering. 13 (2019) 42. https://doi.org/10.1186/s13036-019-0171-6.

[66] C. Dorow, F.-G. Sander, Development of a Model for the Simulation of Orthodontic Load on Lower First Premolars Using the Finite Element Method, Journal of Orofacial Orthopedics / Fortschritte Der Kieferorthopädie. 66 (2005) 208–218. https://doi.org/10.1007/s00056-005-0416-5.

[67] A. Hohmann, U. Wolfram, M. Geiger, A. Boryor, C. Kober, C. Sander, F.G. Sander, Correspondences of hydrostatic pressure in periodontal ligament with regions of root resorption: A clinical and a finite element study of the same human teeth, Computer Methods and Programs in Biomedicine. 93 (2009) 155–161. https://doi.org/10.1016/j.cmpb.2008.09.004.

[68] J. Chen, W. Li, M. V. Swain, M. Ali Darendeliler, Q. Li, M.A. Darendeliler, Q. Li, A periodontal ligament driven remodeling algorithm for orthodontic tooth movement, Journal of Biomechanics. 47 (2014) 1689–1695. https://doi.org/10.1016/j.jbiomech.2014.02.030.

[69] A.M. Schwarz, Tissue changes incidental to orthodontic tooth movement, International Journal of Orthodontia, Oral Surgery and Radiography. 18 (1932) 331–352. https://doi.org/10.1016/S0099-6963(32)80074-8.

[70] A. Hohmann, U. Wolfram, M. Geiger, A. Boryor, C. Sander, R. Faltin, K. Faltin, F.G. Sander, Periodontal Ligament Hydrostatic Pressure with Areas of Root Resorption after Application of a Continuous Torque Moment, The Angle Orthodontist. 77 (2007) 653–659. https://doi.org/10.2319/060806-234.

[71] H.M. Frost, Bone "mass" and the "mechanostat": A proposal, The Anatomical Record. 219 (1987) 1–9. https://doi.org/10.1002/ar.1092190104.

[72] H.M. Frost, A determinant of bone architecture. The minimum effective strain., Clinical Orthopaedics and Related Research. (1983) 286–92.

[73] C. Field, Q. Li, W. Li, M. Swain, Biomechanical Response in Mandibular Bone due to Mastication Loading on 3-Unit Fixed Partial Dentures, Journal of Dental Biomechanics. 1 (2010). https://doi.org/10.4061/2010/902537.

[74] H.M. Frost, A 2003 update of bone physiology and Wolff's Law for clinicians., The Angle Orthodontist. 74 (2004) 3–15. https://doi.org/10.1043/0003-3219(2004)074<0003:AUOBPA>2.0.CO;2.

[75] M. Testa, T. Geri, L. Gizzi, D. Falla, High-density EMG Reveals Novel Evidence of Altered Masseter Muscle Activity During Symmetrical and Asymmetrical Bilateral Jaw Clenching Tasks in People With Chronic Nonspecific Neck Pain, The Clinical Journal of Pain. 33 (2017) 148–159. https://doi.org/10.1097/AJP.0000000000000381.

[76] J. Paphangkorakit, N. Thothongkam, N. Supanont, Chewing-side determination of three food textures, Journal of Oral Rehabilitation. 33 (2006) 2–7. https://doi.org/10.1111/j.1365-2842.2006.01535.x.

[77] J. Martinez-Gomis, M. Lujan-Climent, S. Palau, J. Bizar, J. Salsench, M. Peraire, Relationship between chewing side preference and handedness and lateral asymmetry of peripheral factors, Archives of Oral Biology. 54 (2009) 101–107. https://doi.org/10.1016/j.archoralbio.2008.09.006.

[78] J. Nissan, M.D. Gross, A. Shifman, L. Tzadok, D. Assif, Chewing side preference as a type of hemispheric laterality, Journal of Oral Rehabilitation. 31 (2004) 412–416. https://doi.org/10.1111/j.1365-2842.2004.01256.x.

[79] T.K. Goto, T. Yamada, K. Yoshiura, Occlusal pressure, contact area, force and the correlation with the morphology of the jaw-closing muscles in patients with skeletal mandibular asymmetry, Journal of Oral Rehabilitation. 35 (2008) 594–603. https://doi.org/10.1111/j.1365-2842.2007.01837.x.

[80] M.A. Alkayyal, K.A. Turkistani, A.A. Al-Dharrab, M.A. Abbassy, M. Melis, K.H. Zawawi, Occlusion time, occlusal balance and lateral occlusal scheme in subjects with various dental and skeletal characteristics: A prospective clinical study, Journal of Oral Rehabilitation. 47 (2020) 1503–1510. https://doi.org/10.1111/joor.13095.

[81] B. Koos, A. Godt, C. Schille, G. Göz, Precision of an Instrumentation-based Method of Analyzing Occlusion and its Resulting Distribution of Forces in the Dental Arch, Journal of Orofacial Orthopedics / Fortschritte Der Kieferorthopädie. 71 (2010) 403–410. https://doi.org/10.1007/s00056-010-1023-7.

[82] N.-K. Lee, S.-H. Baek, Stress and displacement between maxillary protraction with miniplates placed at the infrazygomatic crest and the lateral nasal wall: A 3-dimensional finite element analysis, American Journal of Orthodontics and Dentofacial Orthopedics. 141 (2012) 345–351. https://doi.org/10.1016/j.ajodo.2011.07.021.

[83] M.L. Moss, The differential roles of periosteal and capsular functional matrices in orofacial growth, The European Journal of Orthodontics. 29 (2007) i96–i101. https://doi.org/10.1093/ejo/cjl097.

[84] M.L. Moss, L. Salentijn, The capsular matrix, American Journal of Orthodontics. 56 (1969) 474–490. https://doi.org/10.1016/0002-9416(69)90209-7.

[85] B. Sarrafpour, M. Swain, Q. Li, H. Zoellner, Tooth Eruption Results from Bone Remodelling Driven by Bite Forces Sensed by Soft Tissue Dental Follicles: A Finite Element Analysis, PLoS ONE. 8 (2013) e58803. https://doi.org/10.1371/journal.pone.0058803.

[86] S.E.P. Pellizoni, M.A.C. Salioni, Y. Juliano, A.S. Guimarães, L.G. Alonso, Temporomandibular joint disc position and configuration in children with functional unilateral posterior crossbite: A magnetic resonance imaging evaluation, American Journal of Orthodontics and Dentofacial Orthopedics. 129 (2006) 785–793. https://doi.org/10.1016/j.ajodo.2006.02.007.

[87] M. Masi, H.M. Lederman, H.K. Yamashita, L.A. de Arruda Aidar, Temporomandibular joint evaluation with magnetic resonance imaging in children with functional unilateral posterior crossbite, treated with rapid maxillary expansion, American Journal of Orthodontics and Dentofacial Orthopedics. 136 (2009) 207–217. https://doi.org/10.1016/j.ajodo.2007.10.048.

[88] A. Kumar, H. Ghafoor, A. Khanam, A comparison of three-dimensional stress distribution and displacement of naso-maxillary complex on application of forces using quad-helix and nickel titanium palatal expander 2 (NPE2): a FEM study, Progress in Orthodontics. 17 (2016) 17. https://doi.org/10.1186/s40510-016-0131-3.

[89] D.H. Enlow, Facial growth, WB Saunders Company, 1990.

[90] D. Kecik, I. Kocadereli, I. Saatci, Evaluation of the treatment changes of functional posterior crossbite in the mixed dentition, American Journal of Orthodontics and Dentofacial Orthopedics. 131 (2007) 202–215.

[91] Brin, Y. Ben-Bassat, Y. Blustein, J. Ehrlich, N. Hochman, Y. Marmary, A. Yaffe, Skeletal and functional effects of treatment for unilateral posterior crossbite, American Journal of Orthodontics and Dentofacial Orthopedics. 109 (1996) 173–179. https://doi.org/10.1016/S0889-5406(96)70178-6.

[92] H. Gong, M. Zhang, Y. Fan, W.L. Kwok, P.C. Leung, Relationships Between Femoral Strength Evaluated by Nonlinear Finite Element Analysis and BMD, Material Distribution and Geometric Morphology, Annals of Biomedical Engineering. 40 (2012) 1575–1585. https://doi.org/10.1007/s10439-012-0514-7.

[93] K.F. Klein, J. Hu, M.P. Reed, C.N. Hoff, J.D. Rupp, Development and Validation of Statistical Models of Femur Geometry for Use with Parametric Finite Element Models, Annals of Biomedical Engineering. 43 (2015) 2503–2514. https://doi.org/10.1007/s10439-015-1307-6.

[94] H.S. Matthews, A.J. Penington, R. Hardiman, Y. Fan, J.G. Clement, N.M. Kilpatrick, P.D. Claes, Modelling 3D craniofacial growth trajectories for population comparison and classification illustrated using sex-differences, Scientific Reports. 8 (2018) 4771. https://doi.org/10.1038/s41598-018-22752-5.

[95] S. Pirinen, Endocrine regulation of craniofacial growth, Acta Odontologica Scandinavica. 53 (1995) 179–185. https://doi.org/10.3109/00016359509005969.

[96] B. Eslami, H. Behnia, H. Javadi, K.S. Khiabani, A.S. Saffar, Histopathologic comparison of normal and hyperplastic condyles, Oral Surgery, Oral Medicine, Oral Pathology, Oral Radiology, and Endodontology. 96 (2003) 711–717. https://doi.org/10.1016/S1079-2104(03)00379-2.

[97] D.F. López, C. López, M. Moreno, R. Pinedo, Post-Condylectomy Histopathologic Findings in Patients With a Positive 99m Tc Methylene Diphosphonate Single-Photon Emission Computed Tomographic Diagnosis for Condylar Hyperplasia, Journal of Oral and Maxillofacial Surgery. 76 (2018) 1005–1012. https://doi.org/10.1016/j.joms.2017.11.030.

[98] J.M. Reina, J.M. García-Aznar, J. Domínguez, M. Doblaré, Numerical estimation of bone density and elastic constants distribution in a human mandible, Journal of Biomechanics. 40 (2007) 828–836. https://doi.org/10.1016/j.jbiomech.2006.03.007.